Physics of the Earth and Planetary Interiors 370 (2026) 107490

Contents lists available at ScienceDirect

Physics of the Earth and Planetary Interiors

journal homepage: www.elsevier.com/locate/pepi

On the global centroid moment tensor achievements and the next generation earthquake catalogs☆

T.-S. Phạm *, H. Tkalčić, J. Hu, Z. Wei

Research School of Earth Sciences, The Australian National University, Canberra ACT, Australia

ARTICLE INFO

Keywords:
Centroid moment tensor
Inversion
Uncertainty quantification
Source time function
Earth model

ABSTRACT

The systematic determination of the source characteristics of global earthquakes and other seismic sources in a robust and consistent manner is a paramount task in seismology. The Global Centroid Moment Tensor (GCMT) project (Ekström et al., 2012), employing an elegant inversion approach and thoughtful data selection, has been a standard bearer for such an autonomous earthquake catalog. This, by no means an all-encompassing review, celebrates the long-lasting impact and legacy it has left on the seismological and broader Earth science community, from tectonics and structural geology to geodesy and hazard assessment. We also identify and discuss three areas that, in our view, are subject to potential improvement in the current GCMT practice. These include (*i*) enhanced quantification of uncertainty in MT solutions, (*ii*) utilization of 3D Earth models, and (*iii*) robust development of dynamic models that extend beyond a point source assumption in time and space. Recent developments in various areas of theoretical and observational seismology, such as advances in Bayesian inversion, 3D waveform modeling, and applied machine learning methods, will enable the integration of these needed elements into the next generation of routine earthquake catalogs.

1. Introduction

The seismic moment tensor (MT) is a mathematical representation of forces acting in a seismic source under the point source assumption, i.e., the dimension of the ruptured fault is several times smaller than the wavelength of the considered seismic waves (Aki and Richards, 2002; Dziewoński et al., 1981; Gilbert, 1971; Jost and Herrmann, 1989; Julian, 1986). The automatic determination of seismic MTs is of critical importance in seismology due to its unparalleled scientific significance in understanding tectonophysics and mitigating seismic hazards. Several long-standing earthquake catalogs have curated global seismicity at the global scale for several decades, including the International Seismological Centre (ISC – Lentas, 2018; Lentas et al., 2019), U.S. Geological Survey (USGS), and Global Centroid Moment Tensor (GCMT – Dziewoński et al., 1981; Ekström et al., 2012) catalogs. They provide rapid insights into destructive earthquakes and might be significant in minimizing seismic societal impacts.

The centroid moment tensor (CMT) method was introduced by Dziewoński et al. (1981), with the first systematic application to real data by Dziewoński and Woodhouse (1983). A series of publications reported data for several individual years of the catalog in *Physics of the Earth and Planetary Interiors* (e.g., Dziewoński and Woodhouse, 1983; Ekström et al., 2012) and the paper "The global CMT project 2004–2010: Centroid-moment tensors for 13,017 earthquakes" by Ekström et al. (2012) (hereafter, "the 2012 paper") was the latest in the series. In addition to summarizing seismicity in the reported period, the 2012 paper introduced methodological advancements deployed for earthquakes since 2004. That paper and the original CMT paper (Dziewoński et al., 1981) are the recommended citations when using the GCMT catalog via its basic but powerful open-access website www.globalcmt.org. The 2012 paper alone has accrued 2325 citations in Scopus as of May 29th, 2025, reflecting the far-reaching impact of the CMT project on the seismological community and the broader Earth and planetary science community.

This review, although not intended to be exhaustive, celebrates the far-reaching impact of the GCMT project, particularly the publication of the 2012 paper in this journal. The content is structured as follows. Section 2 briefly summarizes the CMT method, updates on statistics of the GCMT catalog, and its limitations. Section 3 highlights areas of impact of the GCMT project on the Earth Sciences community. Sections

☆ This article is part of a Special issue entitled: '55th Anniversary' published in Physics of the Earth and Planetary Interiors.

* Corresponding author.
E-mail address: ThanhSon.Pham@anu.edu.au (T.-S. Phạm).

https://doi.org/10.1016/j.pepi.2025.107490
Received 13 June 2025; Received in revised form 6 December 2025; Accepted 16 December 2025
Available online 23 December 2025

4–6 review forefront research directions, which have the potential to be realized and featured in the next generation of global earthquake catalogs. Section 4 reviews recent progress in quantifying uncertainty, Section 5 reviews efforts to incorporate 3D Earth structures in the CMT inference, and Section 6 features efforts to extend CMT representation beyond a single CMT for large earthquakes.

2. The CMT method and robustness of the global CMT catalog

2.1. Overview of the CMT method

A seismic MT is a force-equivalent model, represented as a symmetric 3-by-3 matrix, of a seismic source under the point-source assumption. The assumption holds when the source dimensions in space and time are several times smaller than the wavelength and period of seismic waveforms under consideration. The six MT parameters, the three spatially-averaged coordinates (i.e., centroid co-latitude, longitude, and depth), and the averaged origin time (centroid) of the seismic source comprise the ten coordinates of a CMT solution. The centroid coordinates refer to the weighted average point in time and space of an extended seismic source. In a pioneering paper, Dziewoński et al. (1981) demonstrated that seismic waveforms can generally place sufficient constraints on ten unknown parameters. This significant finding served as the foundation for the Harvard CMT project, initially managed by the late Professor A. M. Dziewoński for the first 20 years and later by G. Ekström. The project was subsequently relocated to the Lamont-Doherty Earth Observatory of Columbia University, under the leadership of G. Ekström and M. Nettles, in 2006 and was renamed the “Global CMT project” (Ekström et al., 2012).

The CMT method relies on the linear relationship of zeroth order moment tensor, $f_i, i = 1\dots6$, with the observed waveforms, $\boldsymbol{u}^k$,

$$\boldsymbol{u}^k(\boldsymbol{r}t) = \sum_{i=1}^{6} \boldsymbol{G}_i^k(\boldsymbol{r}, \boldsymbol{r}_s, t - t_s)\cdot f_i. \tag{1}$$

In Eq. 1, the bold font denotes vector quantities, while the normal font represents scalars. $\boldsymbol{G}_i^k(\boldsymbol{r}, \boldsymbol{r}_s, t - t_s)$ denotes the Green’s function or the impulse response of the Earth corresponding to the k-th recording components of the elementary MT f_i. A CMT solution consists of six independent MT parameters, spatially average spatial coordinates, and time of the seismic source,

$$\boldsymbol{m} = (f_1, \dots, f_6, r_C, \theta_C, \phi_C, t_C)^T \tag{2}$$

The spatial coordinates in the GCMT convention are the Up (r), South (co-latitude θ), and East (longitude ϕ). The method was introduced by Dziewoński et al. (1981) and subsequently applied systematically to global seismic data in a follow-up study (Dziewoński and Woodhouse, 1983). The CMT solution is derived by minimizing the normalized L2 misfit function between K pair of observed, $\boldsymbol{d}^k$, and predicted, $\boldsymbol{u}^k(\boldsymbol{m})$, waveforms,

$$L(\boldsymbol{m}) = \sum_{k=1}^{K} \frac{\left(\boldsymbol{d}^k - \boldsymbol{u}^k(\boldsymbol{m})\right)^T \left(\boldsymbol{d}^k - \boldsymbol{u}^k(\boldsymbol{m})\right)}{\left(\boldsymbol{d}^k\right)^T \boldsymbol{d}^k}. \tag{3}$$

The Green’s functions, $\boldsymbol{G}_i^k(\boldsymbol{r}, \boldsymbol{r}_S, t - t_S))$, are calculated theoretically by a weighted sum of normal modes (e.g., Gilbert, 1971). The spherically symmetric reference Earth model PREM (Dziewoński and Anderson, 1981) was used for the theoretical calculation with necessary correction for 3D heterogeneity averaged along great circle paths (Dziewoński and Woodward, 1992; Ekström et al., 1997; Woodhouse and Dziewoński, 1984). The construction of a Jacobian matrix $\boldsymbol{A}$ consists of partial derivatives of the theoretical seismograms (Eq. 1) with respect to all CMT parameters,

$$\boldsymbol{A} = \left(\frac{\partial \boldsymbol{u}}{\partial f_1}, \dots, \frac{\partial \boldsymbol{u}}{\partial f_6}, \frac{\partial \boldsymbol{u}}{\partial h_C}, \frac{\partial \boldsymbol{u}}{\partial \theta_C}, \frac{\partial \boldsymbol{u}}{\partial \phi_C}, \frac{\partial \boldsymbol{u}}{\partial t_C}\right)^T. \tag{4}$$

The partial derivatives of the MT elements and centroid time are trivial, thanks to the linear relationship with the waveforms. The partial derivatives of the source coordinates can be computed analytically and cheaply thanks to theoretical seismogram summation. The misfit function can be minimized iteratively using the Newton-Gaussian minimization method with the Jacobian matrix,

$$\boldsymbol{m}^{i+1} = \boldsymbol{m}^i + \left(\boldsymbol{A}^T\boldsymbol{A}\right)^{-1}\boldsymbol{A}^T\left(\boldsymbol{d}^k - \boldsymbol{u}^k\left(\boldsymbol{m}^i\right)\right) \tag{5}$$

where $\boldsymbol{u}^k(\boldsymbol{m}^i)$ represents the forward prediction of the k-th seismogram component computed for the intermediate solution $\boldsymbol{m}^i$. The readers are referred to a more mathematically rigorous description of the CMT method, apart from the original paper (Dziewoński et al., 1981), in more recent papers (e.g., Ekström, 2007; Ferreira and Woodhouse, 2006; Valentine and Trampert, 2012). The iteration typically begins with a preliminary detection from the Preliminary Determination of Epicenters (PDE; U. S. Geological Survey, 2017) bulletin, which has been recently complemented with the events detected using intermediate surface waves (Ekström, 2006). The inversion consists of multiple steps. The interim solution available at the beginning of each step guides a waveform editing procedure, and the minimization is sought with the edited waveforms (Ekström et al., 2012).

The theoretical consideration outlined above is general and can be applied to various types of seismic data. Since 2004, the GCMT project has used three seismic data types to analyze detected events, including body waves, intermediate surface waves, and “mantle waves” (Ekström et al., 2012). Body waves, defined as signals arriving before the minor arc surface waves, are used to constrain the CMT of Mw $\leq$ 7.0, with decreasing weights for larger earthquakes. Intermediate-period surface waves, defined around the prediction of minor arc arrivals, are used for Mw $\leq$ 7.0 events, which are shallower than 300 km. Body waves and surface waves are filtered in a similar frequency band, i.e., between around 50 and 100 s. Mantle waves, filtered at very long periods, typically between 135 and 200 to 300–450 s, with longer periods for larger earthquakes, cover a duration of 0 to 4.5 h from the preliminary origin time. Fig. 1 shows the current snapshot of the Global Seismograph Network (GSN), which provides high-quality, long-period, high-gain seismograms as input for the GCMT inversion. The numbers of stations, components, and shortest periods for each data type are reported in the *ndk* solution format[1] accessed at the catalog website.

The GCMT catalog includes deviatoric CMT solutions – the trace of the CMT is constrained to 0 (Tape and Tape, 2012), with CLVD being the only non-DC component – of 67,270 events between January 1976 and December 2024, as shown in Fig. 2. In 2004, the catalog experienced a sharp increase in the number of admitted events, particularly in the Mw $<$ 5.5 bracket. High-quality surface wave speed maps (Ekström, 2011; Ekström et al., 1997) enabled the incorporation of intermediate-period surface waves (Arvidsson and Ekström, 1998; Ekström et al., 1998), which has markedly increased the convergence rate of CMT solutions in the lowest magnitude bracket (Ekström et al., 2012). In addition to that methodological intervention, the gradual increase in events can be attributed to the growing number of small events being preliminarily reported in the PDE catalog, thanks to the expansion of the global seismographic network. In the meantime, the number of moderate to large events (Mw $>$ 5.5) that can be detected globally has remained relatively stable over the past 50 years of the catalog’s existence. Apart from being a reliable MT catalog, the GCMT also offers a stand-alone moment magnitude, Mw, catalog, and contributes to the depth evaluation of the ISC-EHB catalog (Engdahl et al., 2020).

The CMT method was also adopted to analyze seismic events other than earthquakes. Seismic sources that involve the movement of mass on

[1] https://www.ldeo.columbia.edu/~gcmt/projects/CMT/catalog/allorder.ndk_explained

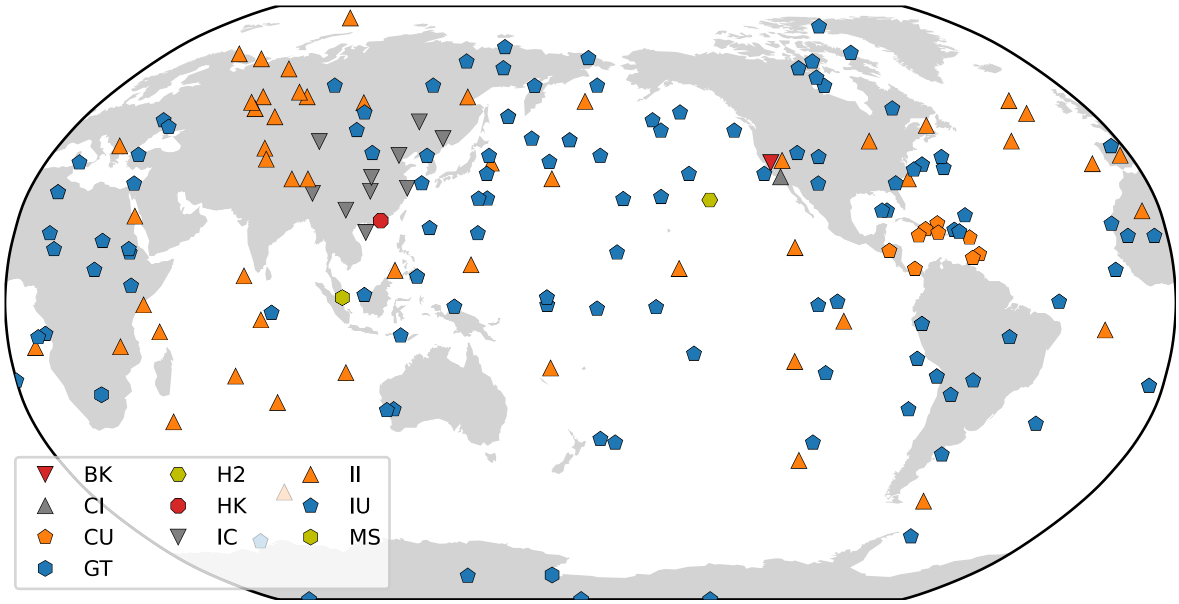

Fig. 1. Map of long-period, high-gain seismic stations included in the global seismographic network (GSN) as of May 2025. The network codes include: BK (Northern California Earthquake Data Center, 2014), CI (California Institute of Technology and United States Geological Survey Pasadena, 1926), CU (Albuquerque Seismological Laboratory (ASL)/USGS, 2006), GT (Albuquerque Seismological Laboratory (ASL)/USGS, 1993), H2 (www.fdsn.org/networks/detail/H2/), HK (www.fdsn.org/networks/detail/HK/), IC (Albuquerque Seismological Laboratory (ASL)/USGS, 1992), II (EarthScope Consortium, 1986), IU (Albuquerque Seismological Laboratory/USGS, 1988), MS (www.fdsn.org/networks/detail/MS/).

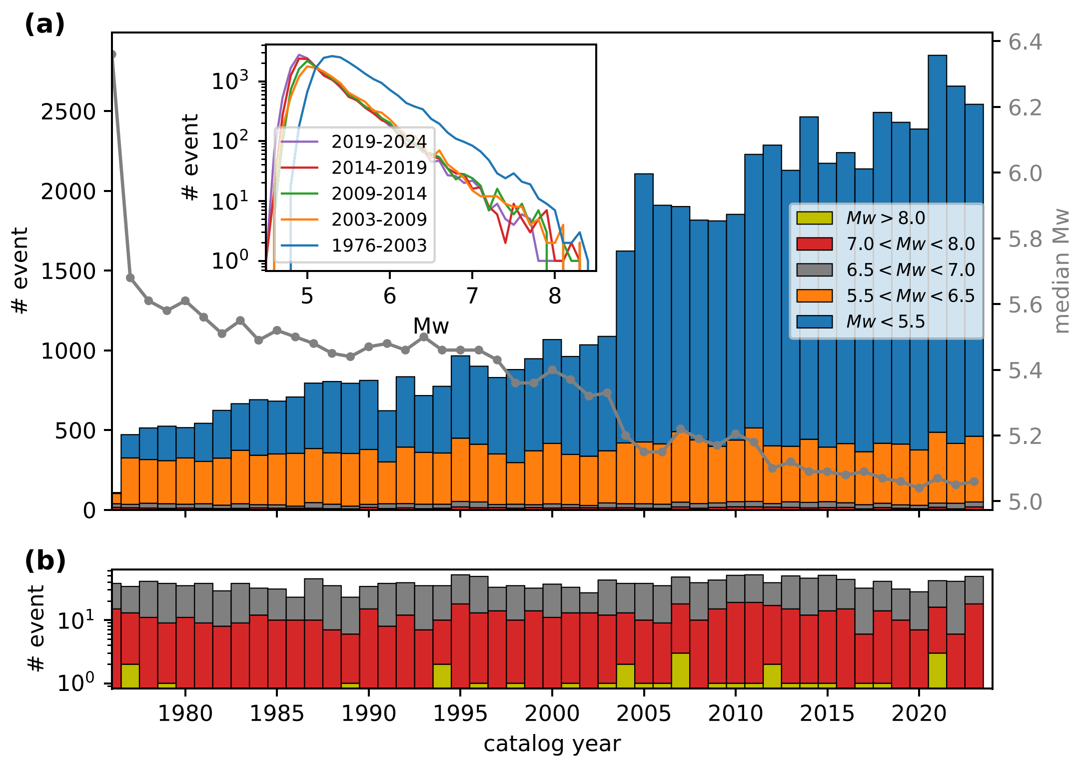

Fig. 2. Overview of the GCMT catalog until December 2024. (a) The main figure shows the growing number of events over the catalog years. Color codes show earthquake magnitude brackets that determine the types and filtering parameters of seismic waveforms to be included in the inversion. The gray line shows the generally decreasing median moment magnitudes as a function of catalog years. In the inset, color lines indicate the distributions of earthquakes as a function of magnitude in several operational periods, with 5-year period bins from 2004. (b) Similar to a) but zooming in Mw > 6.5 earthquakes with the log-scale in the vertical axis for clarity.

the Earth's surface, such as landslides (Kawakatsu, 1989), rockfalls (Gualtieri and Ekström, 2018), seiches (Svennevig et al., 2024), glacial earthquakes (Nettles and Ekström, 2010), or volcanic eruptions (Kanamori and Given, 1982), can often be explained by a single force model more adequately than a double couple focal mechanism. In the centroid single force (CSF) analysis, the six elementary Green's functions, $\boldsymbol{G}_i(\boldsymbol{r}, \boldsymbol{r}_S, t - t_S)$ terms in Eq. 1 need to be replaced by three Green's functions corresponding to three components of a single force, while the minimization strategy is similar to the CMT method (Kawakatsu, 1989; Tsai and Ekström, 2007). The CSF analysis played a crucial role in the discovery and advancing understanding of glacial earthquakes near Greenland's glacier termini (Ekström et al., 2003; Olsen and Nettles, 2017; Tsai and Ekström, 2007; Veitch and Nettles, 2012).

It is worth reminding that the MT routinely obtained by the CMT method is the first-order moment in an infinite series of spatial moments in the expansion of the Earth's response to an earthquake (Julian et al., 1998). The higher-order moment contains information about the orientation and geometry of the failure zone (Clévédé et al., 2004; McGuire et al., 2001; Stump and Johnson, 1982). Recently, Turner et al. (2022) studied the second-order moment of deep earthquakes in the Kuril subduction zone to investigate their rupture propagation. However, the key limitation hindering the broader use of the source representation is its large number of unknowns, which cause inversion instabilities (Julian et al., 1998). The development of exploratory and effective sampling tools, as introduced later in this review, can be helpful in future attempts to pursue this promising direction.

2.2. Effects of unmodelled structural heterogeneity

To retain the efficiency of the forward theoretical seismogram calculation, the Earth's lateral heterogeneity is imperfectly incorporated into the standard GCMT method by the so-called great circle approximation (e.g., Ekström, 2007). A phase correlation term for a source-receiver pair is introduced by averaging phase slowness along the great circle path, which ignores the amplitude effect of the lateral heterogeneity (Ferreira and Woodhouse, 2006). To investigate the potential impact of the assumption on MT inversion, Ferreira and Woodhouse employed a full formulation of surface wave ray theory (Ferreira and Woodhouse, 2007; Woodhouse, 1974) to simulate synthetic waveforms from several 3D Earth models and analyzed the influence on the radiation pattern of very long-period surface waves. As a result, they observed significant variations in recovered focal mechanisms corresponding to different Earth models, and these effects may be smaller when the station coverage is good.

The spectral element method at the global scale (i.e., SPECFEM_GLOBE3D; Komatitsch and Tromp, 2002a, 2002b, Komatitsch and Tromp, 1999) enables full waveform simulation in 3D Earth models. Hjörleifsdóttir and Ekström (2010) generated synthetic waveforms in 3D heterogeneous Earth models (Kustowski et al., 2008; Ritsema et al., 1999) to validate the approximation used to simulate synthetic data for representative Mw 5.5 earthquakes. The study confirmed the small difference with the path-average correction. Earthquake magnitude generally agrees with the 1D Earth model. However, variations from the average crust introduce a slight bias to the estimated Mw, and the 3D structure resulted in a deeper centroid depth than the actual values. These errors were expected to be representative of the solution for the GCMT catalog (Hjörleifsdóttir and Ekström, 2010).

In addition to direct investigations into factors that could contribute to the imperfection of the GCMT catalog discussed in the previous section, another group of studies also reveals some notable statistics about the catalog's overall robustness. Helffrich (1997) and Frohlich and Davis (1999) compared CMT solutions from a set of earthquakes commonly reported in the GCMT, USGS, and ERI catalogs. Both studies found consistency in DC component geometries, confirming the robustness of DC component recovery by the GCMT method. However, the quality of recovered non-DC components is not as well constrained. Rösler and Stein (2022) compiled a catalog of ~8000 earthquakes commonly reported in the GCMT and USGS catalogs. They found the presence of ~20 % of CLVD components in the catalog across a wide range of earthquake magnitudes, fault geometries, and geological settings. The persistently high CLVD component is thus deemed to be artificial, resulting from the inversion process.

The imperfect knowledge of Earth structures, such as isotropic heterogeneity (e.g., Hejrani et al., 2017; Hingee et al., 2011; Rösler et al., 2024b), has been attributed to generating systematic biases in the GCMT catalog. Ma and Masters (2015) demonstrated how earthquake mislocation (standard locations or centroids) can translate into errors in the mapping of azimuthal anisotropy, which, in turn, has also been shown to possibly result in GCMT catalog biases (Kawakatsu, 2024). Section 5 provides a more detailed discussion of the topic.

3. Impact of GCMT on different sub-fields in earth sciences

3.1. Significance in seismology and planetary science

In seismology, the precise source parameters of the GCMT catalog have been instrumental in the development of global seismic models. Seismic waves, generated by earthquakes, travel through the Earth and are recorded by global seismic networks. Structural models of the Earth are developed through seismic tomography, which maps variations in seismic wave speed to reveal features such as subduction zones, mantle plumes, or low-velocity zones. The interpretation of these waves' travel times and amplitudes depends heavily on knowing the exact nature of the seismic source. For instance, Blom et al. (2023) highlighted that errors in earthquake source parameters, including centroid locations, centroid times, and MTs, can significantly influence tomography inversions and affect the interpretation of the resulting models. Without accurate source parameters, it is challenging to distinguish between variations caused by the source and those caused by the Earth's interior structure, which can potentially lead to erroneous models.

3.1.1. Importance for global seismology and regional studies

Many seismic tomography studies rely on moderate to large earthquakes and commonly use GCMT solutions due to their consistency and the unconstrained MTs (not restricted to pure double couples) derived from long-period to very-long-period data (Table 1). For example, Schaeffer and Lebedev (2013) utilized the GCMT catalog to constrain their global shear speed model of the upper mantle and transition zone, highlighting its role in advancing our understanding of Earth's interior structure. This study, with an unprecedentedly large set of waveform fits, improved the resolution of upper mantle features by leveraging GCMT's MT solutions for tomographic models. In regional studies, similarly, Lee et al. (2011) developed rapid full-wave CMT inversions in 3D Earth structure models for Southern California, demonstrating how GCMT methodologies support regional structural models by integrating source parameters with wave propagation simulations. Lloyd et al. (2020) employed source parameters from approximately 240 earthquakes (2007–2016) in the GCMT catalog to perform adjoint inversion for the seismic structure of the Antarctic upper mantle and transition zone. They developed a continental-scale seismic model, ANT-20, which demonstrates significant improvements over existing global and continental-scale tomography models. Wehner et al. (2022) refined the 3-D seismic structure for Southeast Asia—one of the world's most tectonically active regions—using tomography based on data and source parameters from 143 earthquakes (2008–2020) in the GCMT catalog.

Table 1
Key contributions of GCMT to seismology.

Aspect of seismology	Key contribution	Related study
Global Seismic Models	Provides moment tensors for constraining seismic wave speed models	Schaeffer and Lebedev (2013)
Regional Structural Models	Supports rapid full-wave CMT inversions in 3D Earth structure models	Lee et al. (2011); Lloyd et al. (2020); Wehner et al. (2022)
Planetary Seismology	Methodologies adapted for studying seismicity on other planets, such as Mars and the Moon.	Banerdt et al. (2020); Dapré and Irving (2025)

They identified a high-velocity structure beneath Borneo, which may be related to post-subduction processes. Additional global and regional Earth models derived from seismic tomography studies utilizing GCMT solutions are available through the IRIS Earth Model Collaboration (EMC): doi:10.17611/DP/EMC.1.

3.1.2. Importance for planetary seismology

Furthermore, the methodologies developed in the GCMT project have been adapted for planetary science. Banerdt et al. (2020) employed the measure of a cumulative number of events to compare earthquakes and moonquakes with the Martian seismicity detected by the InSight mission on Mars. This paper, which focuses on Mars' seismic activity as of September 2019, draws parallels with Earth's seismic patterns, utilizing GCMT data for comparative analysis and demonstrating its interdisciplinary reach. Building on the similarity between moonquakes and earthquakes, Dapré and Irving (2025) simulated seismic waveforms from various source types—using MTs based on the GCMT catalog—to guide future mission planning for icy moons. Their study recommended optimal landing sites on Enceladus between 20° and 30° from the south pole, where a broad range of seismic phases, including core-transmitted phases sensitive to core properties, could be effectively recorded.

3.2. Significance in geodesy

Geodesy involves measuring and mapping the Earth's shape, gravity field, and orientation, often using techniques such as Global Positioning System (GPS), Interferometric Synthetic Aperture Radar (InSAR), and Satellite Laser Ranging (SLR) to monitor crustal movements and deformations (Table 2). The global consistency of the dataset is crucial for integrating seismic data with geodetic measurements, ensuring accurate models of Earth's surface dynamics.

3.2.1. Importance for crustal deformation modeling

The GCMT project's precise centroid locations and MT solutions are critical for modeling crustal deformations, particularly coseismic and postseismic movements following major earthquakes. For instance, Elliott et al. (2016b) used geodetic data, including GPS and InSAR, to constrain the fault geometry and slip distribution of the 2015 Mw 7.8 Gorkha earthquake in Nepal, which ruptured the Main Himalayan Thrust. While the study primarily focused on geodetic data, it referenced the GCMT catalog for initial source parameters, such as magnitude, focal mechanism, and centroid depth, confirming the thrust faulting consistent with Himalayan tectonics. The catalog's source parameters provide centroid locations essential for modeling crustal deformation fields. Their precision is vital for geodetic applications, such as refining fault models and estimating slip distributions, particularly in regions with sparse seismic networks, ensuring accurate geophysical models for tectonic studies and hazard assessment. The ability to model deformations accurately supports applications such as urban planning, where understanding ground movement is crucial for ensuring the safety of infrastructure.

3.2.2. Role in terrestrial reference frame development

Additionally, the GCMT catalog supports the development of global terrestrial reference frames by providing earthquake source parameters for modeling nonlinear station motions, including coseismic and postseismic deformations. Métivier et al. (2014) utilized GCMT data to compute 20 years of theoretical coseismic ground deformation from successive earthquakes. They assessed their impact on the ITRF2008, the 2008 version of the International Terrestrial Reference Frame, thereby enhancing the frame's precision for geodetic applications, such as GNSS and satellite navigation. Moreover, Altamimi et al. (2016) incorporated GCMT data into the ITRF2014, a new release of the International Terrestrial Reference Frame, to account for postseismic deformations, improving the accuracy of station position time series. Their paper utilized reprocessed time series from four space geodetic techniques (VLBI, SLR, GNSS, and DORIS) to enhance modeling, noting that GCMT data helped model postseismic effects from major earthquakes, resulting in a more robust secular frame and site velocities. These advancements underscore the GCMT project's role in bridging seismic and geodetic datasets, supporting precise positioning systems, navigation, and tectonic assessments, and ensuring that global reference frames remain accurate for applications like satellite tracking and geodynamic studies.

Table 2
Key contributions of GCMT to geodesy.

Aspect of geodesy	Key contribution	Related study
Crustal Deformation Modeling	Provides precise centroid locations and moment tensors for modeling fault slip and postseismic deformation	Elliott et al., 2016a, 2016b
Terrestrial Reference Frame Development	Supplies source parameters for modeling nonlinear station motions due to earthquakes	Métivier et al. (2014); Altamimi et al. (2016)

3.3. Significance in tectonics

Tectonics studies the large-scale motion of Earth's lithosphere, including plate boundaries, fault systems, and mountain-building processes, often driven by earthquakes (Table 3). The GCMT project delivers CMT solutions, which include the earthquake's centroid location, depth, and MT, describing the faulting mechanism (orientation, size, and type, e.g., strike-slip, normal, or thrust). This global, consistent dataset is crucial for interpreting seismic data to map tectonic structures and understand Earth's dynamic processes.

3.3.1. Importance for fault mapping

GCMT data are vital for fault mapping, as MTs help identify the type and orientation of faults, which are crucial for delineating tectonic structures. For instance, the MT's principal axes indicate whether faulting is thrust, normal, or strike-slip, providing insights into fault geometry. This is essential for mapping fault systems globally, from mid-ocean ridges to continental interiors, thereby aiding in the understanding of tectonic fabric and deformation patterns. Olive et al. (2024) analyzed 125 seismic events on the northern Mid-Atlantic Ridge (from 26 September 2022 to 30 January 2023) and 47 events on the Carlsberg Ridge (from 10 August 1990 to 14 June 2019) using the GCMT method and its solutions. They identified sequences of reverse-faulting earthquakes occurring approximately 15 km off-axis on both ridges. Mid-ocean ridges have traditionally been considered purely extensional environments. However, the detection of reverse-faulting events in this study reveals the presence of active compressive forces, indicating ongoing tectonic shortening. These findings underscore the dynamic and complex nature of plate boundary processes at mid-ocean ridges.

3.3.2. Role in plate boundary studies

Plate boundary studies benefit from GCMT data (and its predecessors in the early stages of the plate tectonics theory) by analyzing earthquake distribution and mechanisms, which help delineate plate boundaries and understand their interactions. For example, at transform boundaries,

Table 3
Key contributions of GCMT to tectonics.

Aspect of tectonics	Key contribution	Related study
Plate boundary studies	Delineate plate boundaries and understand their interactions	Baxter et al. (2020)
Fault System Mapping	Identifies fault types and orientations for tectonic structure mapping	Olive et al. (2024)
Subduction Zone Geometry	Constrains slab geometries using intraslab earthquake data	Hayes et al. (2018)
Tectonic Strain and Stress Analysis	Estimate regional stress state and the accumulation of strain	Li and Gurnis (2024)

such as the San Andreas or the Anatolian faults, GCMT data reveal strike-slip mechanisms, whereas, at convergent boundaries, thrust mechanisms indicate subduction or collision. This helps model how plates interact, whether through subduction, collision, or transform motion, enhancing our understanding of plate tectonics. Baxter et al. (2020) analyzed 492 CMTs of shallow earthquakes from the GCMT catalog within the Lau Basin, comparing their orientations to mapped seafloor lineaments. They inferred the strike, dip, and dip direction for 308 faults and identified the fault type for 258 additional structures. Their results suggest that the northern boundary of the Niuafo'ou microplate follows a transform that links the Mangatolu Triple Junction to a nearby ridge while its southeastern boundary remains evolving. They also propose a new plate boundary within the Tonga Plate, potentially forming a new triple junction near the Fonualei Rift and Spreading Center, as well as the Fonualei discontinuity.

3.3.3. Contribution to subduction zone geometry

Subduction zones, where one plate is forced under another, are critical in tectonics, and GCMT data are essential for constraining their geometries. For example, Hayes et al. (2018) developed the Slab2 model, a comprehensive geometry model detailing 24 million square kilometers of subducted slabs from the ocean trench to the upper mantle, which relies on GCMT data for earthquake hypocentres and focal mechanisms. Intraslab earthquakes, along with their MTs, help map the slab's shape and depth, revealing stress within the slab and aiding in the understanding of subduction processes, which is crucial for seismic hazard assessment in populated regions.

3.3.4. Role in tectonic strain and stress analysis

GCMT data contributes to tectonic strain and stress analysis by providing information on faulting styles, which relate to regional stress fields and the accumulation of strain. The MT components indicate the style of faulting (e.g., thrust for compression, normal for extension), offering insights into how tectonic stress is accommodated. This is crucial for understanding strain partitioning at plate boundaries and within deforming zones, aiding in models of long-term tectonic evolution. Li and Gurnis (2024) utilized the CMTs of shallow earthquakes ($Mw > 5$, depth < 30 km) from the GCMT catalog to directly estimate the present-day stress state in the Puysegur region, a well-constrained example of subduction initiation offshore South Island, New Zealand. Focal mechanism fault types indicate a predominantly compressional to transpressional stress regime across the region, with strike-slip faulting prevailing near the Snares Zone. Integrating these results with other observations, they suggest that subduction initiation in this area involves rapid strain weakening characterized by a small critical displacement.

3.4. Significance for seismic hazard assessment

High-quality source parameters from the GCMT are essential for seismic hazard assessment, particularly for understanding the potential for large earthquakes on major faults. For example, Elliott et al. (2016a) studied the 2015 Mw 7.8 Gorkha earthquake in Nepal, which ruptured the Main Himalayan Thrust (MHT), using geodetic data to constrain fault geometry. While not directly citing GCMT for geometry, the catalog provides source parameters like magnitude, focal mechanism, and centroid depth, confirming thrust faulting consistent with Himalayan tectonics. This information is vital for assessing seismic hazards, informing building codes, and disaster preparedness in tectonically active regions. Bird et al. (2015) used shallow earthquakes from the GCMT catalog (1977–2004), in combination with the Global Strain Rate Map (version 2.1), to develop the Global Earthquake Activity Rate model 1 (GEAR1). They then cross-validated the model using earthquake data from the 2005–2012 GCMT catalog. GEAR1 estimates the rate of shallow earthquakes with magnitudes ranging from 6 to 9 worldwide. It serves as an essential tool for seismic hazard assessment, particularly in regions lacking dedicated national or regional hazard programs. Additional global and regional seismicity models that incorporate GCMT data are discussed in Bayona et al. (2021).

3.5. Broader interdisciplinary impact

The GCMT project's influence extends beyond traditional geophysics fields, such as global seismology and tectonics, with its data and methods applied in computational geophysics and engineering. Its open-access nature has democratized seismic data, enabling machine learning studies that predict earthquake magnitudes and support real-time hazard systems. The catalog's standardized format has been adopted in regional catalogs, such as the European-Mediterranean RCMT (http://rcmt2.bo.ingv.it/) and InaCMT (Nakano et al., 2010), further illustrating its versatility.

3.6. Critical perspective and legacy

While the GCMT catalog is a gold standard, potential biases in regions with sparse seismic networks, as noted in tectonic studies, suggest areas for improvement. For example, Hingee et al. (2011) laid the groundwork for advanced continental-scale MT inversions by developing a methodology to incorporate 3D structural models for earthquakes in the Australian region. It critically demonstrated that accounting for 3D Earth heterogeneity significantly improves the accuracy of CMT solutions compared to traditional 1D models, particularly in regions with complex crustal structures. By using a 3D velocity model, the study achieved better waveform fits and more reliable source parameters, setting the stage for the subsequent work of Hejrani et al. (2017), which further refined CMT catalogs for tectonically active areas such as Papua New Guinea and the Solomon Islands. This approach highlighted the necessity of 3D models to capture lateral heterogeneities. From a critical perspective, Hejrani et al. (2017) emphasized that 1D Earth models often oversimplify seismic wave propagation, resulting in inaccurate centroid locations and MT solutions, particularly in tectonically complex regions with significant lateral heterogeneities. Incorporating 3D velocity models challenges the reliance on simplified models, emphasizing that 3D structures are necessary to capture the true complexity of seismic wave paths and enhance the accuracy of earthquake characterizations, particularly in subduction zones.

Because the GCMT catalog relies on long-period body and surface waves, which provide limited resolution for depth, the minimum centroid depth is fixed at 12 km. Additionally, since it depends on data from the global seismic network, the catalog may miss events with poor signal-to-noise ratios or inadequate station coverage—cases where regional CMT solutions are often more reliable. Furthermore, the paper's focus on deviatoric moment tensors may limit its ability to capture non-tectonic sources, although its adaptability, as seen in planetary applications, mitigates this limitation.

Its legacy, with over 2325 citations, underscores its role in driving scientific progress, from understanding Earth's interior to enhancing Mars exploration. In conclusion, the Ekström et al. (2012) paper has had a lasting impact on geophysics and related fields, providing a robust foundation for studying earthquakes, Earth's structure, and seismic hazards. Its methodological innovations and comprehensive data have enabled significant advancements in seismology, tectonics, geodesy, and hazard assessment, as well as applications in planetary science. The paper's influence is evident in its extensive citation record and its role in shaping current and future research directions.

4. CMT inversion with uncertainty quantification

The ultimate goal of the standard GCMT method is to find the CMT solution that produces the lowest misfit (Eq. 3) between the observation and the predicted waveforms, which are synthesized with a set of subjective choices, such as the 1D radial representation description of the

Earth's interior and how the waveforms are predicted. The CMT project reported the "standard error" of estimated parameters using the error propagation procedure, assuming Gaussian uncorrelated data noise (Valentine and Trampert, 2012). The estimates appear to be unrealistically conservative, as they do not account adequately for data noise correlation and possible forward theory (Duputel et al., 2012). As a consequence, Rösler et al. (2021), when comparing common CMT solutions independently reported by the GCMT and USGS catalogs, found that the quoted standard errors could be an order of magnitude smaller than they possibly are. They attributed the difference to possible artifacts relating to subjective choices made in the catalogs' inversion procedures.

Similar to any inverse problem, the MT inversion is generally subjected to two sources of uncertainty: data noise and theory error, which are responsible for residuals between observed and predicted waveforms (Duputel et al., 2012; Tarantola and Valette, 1982). Data noise is involved in signal acquisition, which interferes with the earthquake-induced signals, including, not only limited to, background ambient noise and instrumental glitches. Theory errors originate from assumptions underlying the forward problem solver, including imperfect knowledge of the Earth's elastic or anelastic structures, source mislocation, or simplifications in the mathematical representation of the seismic source or wave propagation. Among factors of theory errors, uncertainties corresponding to the imperfect Earth structures, also referred to as Green's function errors or structural errors, are considered to be most significant, yet usually not adequately considered in MT inversion studies (for more on this topic, see, e.g., Hallo and Gallovič, 2016; Rösler et al., 2024b; Yagi and Fukahata, 2011).

In geophysical inference, the Bayesian approach has proven to be a powerful tool for quantifying uncertainty (e.g., Aster et al., 2013; Dettmer and Dosso, 2012; Tarantola, 2005; Valentine and Sambridge, 2023; Zahradník and Sokos, 2025). In this framework, both the unknown model, $\boldsymbol{m}$, and the observed data vector, $\boldsymbol{d}_{obs}$, are considered as stochastic variables. The Bayes' theorem of conditional probability is expressed as follows,

$$p(\boldsymbol{m} \mid \boldsymbol{d}_{obs}) \propto p(\boldsymbol{d}_{obs} \mid \boldsymbol{m}) \cdot p(\boldsymbol{m}) \tag{6}$$

where the posterior probability, $p(\boldsymbol{m} \mid \boldsymbol{d}_{obs})$, is proportional to the likelihood, $p(\boldsymbol{d}_{obs} \mid \boldsymbol{m})$, multiplied by the prior, $p(\boldsymbol{m})$. An ensemble of solutions is then sampled from the model space using various Markov Chain Monte Carlo sampling methods (e.g., Betancourt, 2018; Del Moral et al., 2006; Dettmer and Dosso, 2012; Goodman and Weare, 2010; Roberts and Rosenthal, 2001) to realize the posterior probability as it often does not have an analytical form. The inverted solution and its associated uncertainty can be estimated empirically from the solution ensemble.

The likelihood, $p(\boldsymbol{d}_{obs} \mid \boldsymbol{m})$, is where the forward prediction, $g(\boldsymbol{m})$, is quantitatively compared with the observation under certain assumptions on the probabilistic distribution of their difference. It is common in geophysical inverse problems to assume the mismatch between the data and predicted waveforms complies with a multivariate Gaussian distribution characterized by a covariance matrix, $\boldsymbol{C}_D$. As such, the likelihood function is defined as follows,

$$p(\boldsymbol{d}_{obs} \mid \boldsymbol{m}) = \frac{1}{(2\pi)^N \sqrt{|\boldsymbol{C}_D|}} \exp\left(-\frac{1}{2} (\boldsymbol{d}_{obs} - g(\boldsymbol{m}))^T \boldsymbol{C}_D^{-1} (\boldsymbol{d}_{obs} - g(\boldsymbol{m})) \right) \tag{7}$$

In practice, it is often assumed for convenience that both data and theory noise comply with the Gaussian distribution characterized by covariance matrices, $\boldsymbol{C}_d$ for data noise, and $\boldsymbol{C}_t$ for theory error. As such, the aggregated error also has a Gaussian distribution with a covariance matrix added from the two, $\boldsymbol{C}_D = \boldsymbol{C}_d + \boldsymbol{C}_t$ (Duputel et al., 2012; Phạm and Tkalčić, 2021; Tarantola, 2005; Tarantola and Valette, 1982). Active research directions have focused on developing a different form of the covariance matrix to better represent the nature of each error type or even bypassing the Gaussian likelihood assumption. Below, we reviewed works representing such directions.

4.1. Correlated data noise

Full-waveform data noise is correlated, meaning the noise amplitude at a point in time is likely dependent on that acting at adjacent times. This is due to a number of factors, including the presence of correlated ambient noise field (e.g., Shapiro et al., 2005), the local structure effects embedded in the temporal recordings (e.g., Tauzin et al., 2019), and the necessary bandpass filter applied to waveforms for revealing desired signals (e.g., Ekström et al., 2012).

Most studies have attempted to use a functional form of covariance matrices, aiming to represent the statistical nature of data noise. Duputel et al. (2012) employed a decaying exponential formulation, emphasizing the importance of utilizing a non-diagonal data covariance matrix to account for the temporal correlation of seismic noise. Mustać and Tkalčić (2016) later proposed the use of two attenuated cosine functions for the correlated noise model, whose parameters are empirically estimated from noise records of seismically quiet days. Instead of modeling the data noise with a closed function form, Vackář et al. (2017) and Mustać et al. (2018) proposed using pre-event noise records to estimate the data noise covariance matrices.

Most recently, Saoulis et al. (2025) introduced a simulation-based inversion (SBI) framework for full-waveform MT inversion. In this framework, the likelihood function, requiring a Gaussian distribution of seismic noise, is voided. Instead, the authors employed a deep-learning network, the neural density estimator (Alsing and Wandelt, 2019; Dinh et al., 2016; Papamakarios et al., 2017), to directly learn the complex distribution in the joint space of MT parameters and observed data, using synthetic waveforms with real noise added. The novel approach, which utilizes deep-learning methods in geophysical inversion, could be welcomed in a wide range of seismological applications.

4.2. Forward theory error

In MT inversion, the forward waveform simulation is subjected to various assumptions to be more tractable. One of the typical assumptions is to use a 1D velocity model to represent the heterogeneity of the Earth's interior. In the standard GCMT method, 3D heterogeneity is accounted for by correcting path-averaged structures using high-resolution surface wave velocity maps (Ekström et al., 1997). In local and regional applications, where short-period surface waves (often shorter than 50 s) are used, the 3D heterogeneity introduces significant station-specific phase shifts, which can compromise the potential waveform fit (Hu et al., 2023). To account for the effect of 3D structures, the time shifts between observed and synthetic waveforms are often relaxed. The misfit is evaluated on the residual when the waveforms are optimally aligned using the maximal correlation lapse time. This approach is widely applied in the family of cut-and-paste methods (e.g., Wang and Zhan, 2020; Zhao and Helmberger, 1994; Zhu and Helmberger, 1996), where MT parameters are grid-searched for the minimal misfit, allowing for time shifting (Alvizuri and Tape, 2018; Takemura et al., 2020; Thurin et al., 2025).

The station-specific time shifts between observed and synthetic data reflect information about the local geology along each source-receiver path (e.g., Alvizuri and Tape, 2018; Dreger et al., 2021). Thus, the joint inversion of the time shifts with MT parameters is considered a simplified approach to mitigating structural errors. Phạm (2024) cast an optimization inverse problem for MT parameters and station-specific time shifts, where the misfit function is minimized using modern infrastructure in deep learning frameworks. More comprehensive approaches involve Bayesian sampling in the joint MT and time-shift parameter space, which can significantly increase computational time due to the enlarged parameter space (Hu et al., 2024; Hu et al., 2023; Vasyura-Bathke et al., 2020; Viltres et al., 2021).

In the Bayesian framework, a rigorous treatment of theory error involves an additive term, $\boldsymbol{C}_t$, to the data noise covariance matrix, $\boldsymbol{C}_d$. Duputel et al. (2012) considered the centroid mislocation as a source of theoretical error of W-phase CMT inversion for large earthquakes. This study demonstrated two methods to construct the theory error covariance matrix. The first approach employed the Monte Carlo sampling method to generate an ensemble of simulated waveforms corresponding to the random source locations drawn randomly from a prior distribution. The theory error covariance matrix is then estimated empirically from the waveform ensemble. Secondly, they proposed an alternative method to approximately represent the theoretical uncertainty and avoid the expensive Monte Carlo simulation. The two approaches to modeling the theoretical error yielded similar results in the examined test cases.

The imperfect knowledge of the Earth's structure is the most significant source of forward theory error and has, therefore, received considerable attention from some research groups. The imperfect Earth structure (structural error) resulted in imperfect Green's functions, and so it is also often referred to as Green's function uncertainty (Hallo and Gallovič, 2016; Yagi and Fukahata, 2011). It is noted that the structural covariance matrix, $\boldsymbol{C}_t(\boldsymbol{m})$, depends on the induced MT (Duputel et al., 2012; Phạm and Tkalčić, 2021; Vasyura-Bathke et al., 2021). For example, unlike data noise, which remains independent from earthquake magnitudes (Duputel et al., 2012), the amplitude of structural errors increases with event magnitudes. The influence of structural errors on waveforms at receivers located on the nodal plane is smaller than that falling near the tension or traction axes.

Similar to the consideration of centroid mislocation featured in Duputel et al. (2012), there are two methods to calculate the structural error covariance matrix. The first approach, which estimates the structural error covariance matrix from waveform ensembles corresponding to randomly perturbed Earth models (e.g., Hallo and Gallovič, 2016; Vasyura-Bathke et al., 2021), is computationally expensive, especially in 3D (Phạm et al., 2024; Poppeliers and Preston, 2020). In addition, several critical yet subjective assumptions must be made regarding the spatial distribution properties of the velocity model error, such as whether the errors are spatially uncorrelated or how large the perturbation magnitude is. Phạm et al. (2024) demonstrated that such choices have a significant impact on the performance of the estimated structural matrices. Chiang et al. (2025) suggested embracing objectivity by using data-derived distributions of velocity models and source locations, but such information is not always available (Scheiter et al., 2022).

To avoid the computational simulation expenses and the required subjectivity, several studies proposed simplified error models to capture the dominant effects of structural errors on the simulated waveforms (Yagi and Fukahata, 2011). For example, Hallo and Gallovič (2016) proposed a lightweight version of the theory's covariance matrix by employing the observation that temporal shifts of seismic signals primarily dominate the structure errors. Vasyura-Bathke et al. (2021) promoted a slightly different approach to constructing a covariance matrix, aiming to represent the joint effect of data noise and structure error. The ensemble of waveform residual between the observation and predicted waveforms from a preliminary MT solution is sampled. The sampled residuals are used to feature an empirical non-Toeplitz covariance matrix, which is claimed to adequately represent both data and theory errors. In our view, the simplified covariance matrix estimation commonly fails to embrace the above-noted dependence on the induced MT, which is also the actual MT solution. Thus, their performance in real applications should be further examined (Phạm et al., 2024).

Despite the exerted efforts, incorporating the structural error in MT inversion remains a challenging research topic awaiting breakthroughs. This is partly due to the inadequate representation of uncertainty in published Earth models in the past. So far, efforts have been focused on proving the concepts on local-scale applications, while global-scale studies, to our knowledge, are yet to be approached. Research in properly characterizing the statistical distribution of waveforms induced by velocity model uncertainty is particularly welcome, as the Gaussian distribution has been commonly used primarily due to its convenience. A likelihood-free approach similar to the simulation-based inversion previously demonstrated for data noise (Saoulis et al., 2025) has the potential for further investigation.

4.3. Shallow source ambiguity

Another significant source of uncertainty lies in the difficulty of resolving several specific source types at shallow source depths. First, the dip-slip focal mechanisms, such as $M_{r\theta}, M_{r\phi}$ excite low-amplitude seismic waveforms relative to other MT components (Dziewoński et al., 1981), resulting in the unstable recovery of the components from seismic waveforms (Dahlen and Tromp, 1998). Accurately modeling wave propagation in 3D structures at high frequencies is crucial for better resolving seismic source components (e.g., Ferreira and Woodhouse, 2006; Hejrani and Tkalčić, 2020; Mustać et al., 2020; Takemura et al., 2020).

The second type of well-known seismic source ambiguity is often encountered in non-DC source types. At source depths that are shallow relative to the signal dominant wavelengths, isotropic source and vertical CLVD produce nearly identical long-period waveforms for surface waves at regional scales (Alvizuri and Tape, 2018; Ford et al., 2010; Kawakatsu, 1996). The incorporation of body waves (waveforms or polarities) at teleseismic distances helps address the ambiguity, as the two source types result in P-wave arrivals with opposite polarities (Chiang et al., 2014; Dreger et al., 2021; Ford et al., 2012).

5. Incorporation of 3D Earth models in CMT inversion

A critical factor affecting the accuracy and robustness of MT inversion is the quality of the predicted seismograms used in the inference. In the standard GCMT method, analytical waveforms of a 1D reference Earth model were used for a cheap calculation and reasonable approximation at long periods. However, thanks to the increasing availability of seismic data, efficient numerical solvers, seismic tomography methods, and computational resources, our understanding of the Earth's internal structures has evolved significantly, as represented by high-quality 3D Earth models across various scales (e.g., Fishwick and Rawlinson, 2012; Kim et al., 2016; Lei et al., 2020; Simutė et al., 2016). Thus, incorporating 3D Earth structures in MT inversion is expected to improve the quality of predicted waveforms, especially in geologically complicated regions, such as subduction zones or volcanic areas. The improved capacity for waveform modeling will also be helpful when inverting for smaller or older earthquakes with only a few seismograms.

Despite the increasing availability and efficiency of advanced software packages (Gokhberg and Fichtner, 2016; Maeda et al., 2017; Sjögreen and Petersson, 2012; Tromp et al., 2008), numerical simulations of seismic waveforms in a 3D Earth model remain a significant computational challenge. The physics-informed Neural Network approach (e.g., Rasht-Behesht et al., 2022), once successfully demonstrated, has the potential to dramatically reduce the computational expense associated with 3D waveform modeling. Research development has focused on devising practical and efficient routines for 3D MT inversion that could be deployed for a larger number of events in an automatic manner. Here, we discuss some notable 3D MT inversion studies from the last two decades, which can be grouped into two thematic categories depending on whether the partial derivatives of the ten CMT parameters for the forward waveforms are available.

5.1. Derivative-based inversion approach

At the local scale, Liu (2004) aimed to utilize the high-resolution 3D structure of southern California (Süss and Shaw, 2003) to systematically determine source parameters for events in the region. Following an inversion approach similar to the standard GCMT method, their procedure evaluated numerically the Jacobian matrices (Eq. 4), which involved 10 computationally expensive 3D simulations for individual events. Later, Kim et al. (2011) proposed an adjoint method for CMT inversion, which reduced the number of simulations per earthquake to two. However, they demonstrated that the point source is ill-suited when backpropagating the residual in structures of the Earth's interior that are not sufficiently well understood (Sawade et al., 2022).

Due to the computational expense of on-the-fly forward simulations, later studies often preferred to use pre-computed Green's function databases, leveraging the reciprocity property (Eisner and Clayton, 2001) of the seismic wavefield to speed up the inversion. Instead of simulating the seismic wavefield from a trial source location (Fig. 3a), the strain wavefield induced by single force sources located at each of the selected station locations is saved at spatial grid points covering the source region of interest (Fig. 3b). The saved strain waveforms, according to the reciprocity theorem, are equivalent to the waveforms where the actual source and receiver pair are exchanged. Thus, the forward double-couple waveform can be computed effectively by numerically differentiating the single-force waveforms between two adjacent points to the source location of interest (e.g., Hejrani et al., 2017).

Several author groups intervened with numerical solvers to store the complete interpolation parameters used in the forward simulation into files, albeit at the cost of large storage volumes. This ensures the complete reproduction of the wavefields and their partial derivatives from the pre-computed parameters at high precision (Sawade et al., 2025; Sawade et al., 2022; Simutė et al., 2023). Hence, they can approach the CMT inverse problem using derivative-based approaches. At the regional scale, Simutė et al. (2023) investigated the CMT inversion of earthquakes offshore the Japanese islands using a 3D Earth model previously constructed through full-waveform simulation with regional earthquakes (Simutė et al., 2016). The authors customized their group's spectral element method code for waveform simulations in a regional 3D model, SES3D (Gokhberg and Fichtner, 2016), to build a full strain wavefield reciprocal database. Thanks to the comprehensive preparation, the authors could approach the CMT inversion in the Bayesian framework using the derivative-based Hamiltonian Monte Carlo sampler, with the effectiveness benchmarked in a proof-of-concept study (Fichtner and Simutė, 2018).

At the global scale, Sawade et al. (2022) sought to extend the standard CMT method by employing a dataset of Green's functions pre-computed for the GLAD-M25 model (Lei et al., 2020). The model, a recent update from its predecessor (Bozdağ et al., 2016), was constructed using the adjoint method, fitting a global collection of seismic waveforms. Both of the global models used the GCMT catalog as input,

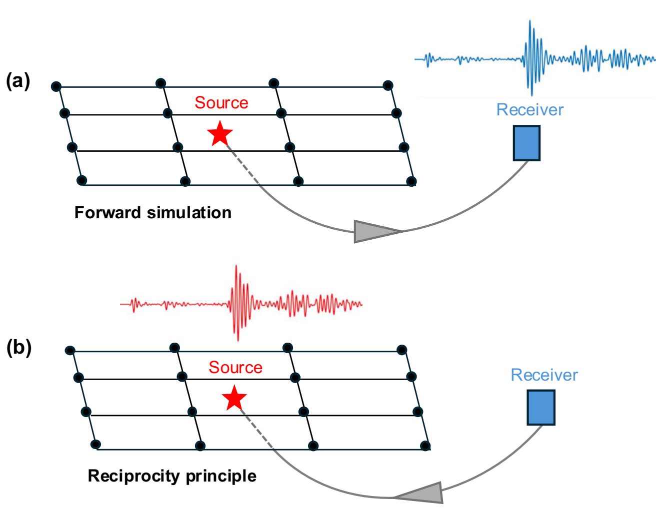

Fig. 3. Reciprocity approach in the centroid moment tensor inversion based on the 3D model. (a) Forward simulation. (b) source-receiver reciprocity approach.

so they were chosen to ensure compatibility (Valentine and Woodhouse, 2010). Similar to Simutė et al. (2023), the complete reciprocal wavefields, pre-computed by SPECFEM_GLOBE3D (Komatitsch and Tromp, 2002a, 2002b), are saved to disk for station locations of the GSN network. The optimal solution is also derived using an iterative procedure (Eq. 5), similar to the standard GCMT method. The resultant GCMT3D catalog comprises 9382 events, which are re-analyzed from a subset of the GCMT catalog. Rösler et al. (2024a) confirmed that the catalogs are highly compatible despite arguable discrepancies due to the use of 1D and 3D earth models. More recently, Sawade et al. (2025) introduced the parsimonious 3D Green's function database, which promises a step toward automating the GCMT3D procedure.

5.2. Derivative-free inversion approaches

Derivative-free inversion approaches are technically simpler, as a dataset of Green's functions for the 3D Earth model of the source region can be computed at a sparse grid covering the source region of interest using the aforementioned reciprocity theorem (Eisner and Clayton, 2001). As spatial derivatives are not available for optimization, a grid search is often performed in the high-dimensional parameter space to identify the best-fitted CMT solution. In practice, several specific variations are employed by different groups to accelerate the search. An example is to combine the grid search for non-linear parameters, such as source location and centroid time, with linearly inverted MT at each visited source location and origin time. The intrinsic weakness of this approach is the lack of objective means to assess the uncertainty of the inverted parameters.

Hingee et al. (2011) demonstrated the significant effect of 3D earth structures in the Australasian region, utilizing the AMSAN.19 model (Fichtner et al., 2010; Fichtner et al., 2009) and the 3D attenuation model. Hejrani et al. (2017) expanded the effort by building a comprehensive 3D green function database for earthquakes in the region north of Australia, i.e., Papua New Guinea and the Solomon Islands, using a set of stations primarily located on the Australian continent. The work resulted in a new earthquake catalog, CSCMT-3D, comprising 318 earthquakes with more centroid constraints at shallow depths than the default depth of 12 km for shallow events in the GCMT. More significantly, the 3D catalog exhibits systematically higher DC components than those in the GCMT catalog, which is expected for tectonic earthquakes in a tectonically active region.

Takemura et al. (2020) applied the framework to moderate-sized earthquakes, utilizing both onshore and offshore seismic stations to investigate the slip distribution along the plate boundary in the Nankai Trough offshore Japan. They demonstrated that a 3D earth model significantly enhances the reliability of the dip angle and centroid location in such complex subduction zone structures. Similarly, Wang and Zhan (2020) developed a waveform-based approach to automatically determine the focal depth and MT of small-to-moderate earthquakes by combing gCAP3D (Zhu and Zhou, 2016), the SGT method (Zhao et al., 2006) and a high-quality 3D earth model of Southern California obtained by scattering-integral and adjoint-wavefield method (Lee et al., 2011). They found that the application of an accurate 3D model significantly reduces the moment tensor uncertainties, leads to more accurate focal depths and moment magnitudes, and reduces the bias in the fractions of non-double-couple components caused by using a 1D model.

In addition, incorporating rotational ground motion into the source inversion based on a 3D model can further enhance the accuracy of determining source parameters. Donner et al. (2020) applied a Bayesian inversion strategy to test the feasibility of combining 6C data (three components of translational ground motion and three components of rotational ground motion) with 3D Green's functions to improve the resolution of the seismic moment tensor based on a nuclear event and a tectonic event in Korean Peninsula. They found that rotational ground motion can help better constrain the isotropic part of the source at higher frequencies as the influence of rotational motions increases with frequency.

6. Extended MT inversion in time and space

In the standard GCMT method, seismic sources, regardless of their size, are approximated as a moment tensor located at the centroid location under the point source approximation. The source half-time duration is estimated a priori from its scalar moment rather than being inferred from waveform data (Ekström et al., 2012),

$$t_{hdur} = 1.05 \times 10^{-8} M_0^{1/3} \tag{8}$$

The approximation holds when the seismic source dimensions in time are several times smaller than the wavelengths and periods of the considered signals. For mega-earthquakes that occur in extended fault zones or when relatively short-period signals are considered, the approximation conditions no longer hold (Tsai et al., 2005). Representation of seismic sources that extend beyond the point-source assumption, such as using multiple CMTs or incorporating moment rate functions, also known as source time functions (STFs), has been considered a transitional step toward finite source representations (Vallée et al., 2011). Here, we will review several recent attempts at the former two approaches in further detail.

To address one of the limitations of standard CMT inversion, which approximates the source as a single point in space and time, the multi-CMT source representation has been developed. Instead of assuming a single CMT source, this method uses a series of CMTs to represent the complex rupture process of an earthquake. Tsai et al. (2005) originally developed this approach to study the great Sumatra earthquake of December 26, 2004, which ruptured a nearly 1200 km long fault in ~600 s (e.g., Ammon et al., 2005). They iteratively introduced a composite source of from one to six independent CMTs to fit recorded mantle waveforms and used statistical analysis to determine the optimal number of CMTs. In their implementation, the depth of each source was fixed due to the limited constraints from long-period mantle waves.

Zhan et al. (2014) and Jia et al. (2020) presented a subevent inversion approach in which the centroid locations, centroid times, durations, and MTs of all subevents are determined through a combination of nonlinear and linear inversion techniques. A key distinction in Jia et al. (2020) is the incorporation of pP waveforms to constrain the depth of each subevent better. This multi-CMT method is particularly well-suited for investigating complex rupture dynamics in large earthquakes. Jia et al. (2022) applied the subevent inversion approach to investigate the rupture process of the 12 August 2021 Mw 8.2 South Sandwich Islands earthquake. Their analysis revealed a complex rupture sequence involving multiple subevents, including a silent and predominantly slow subevent in the middle that connects a regular deep thrust subevent at the beginning to two additional regular thrust subevents at the end. More recently, Jia et al. (2023) used subevent inversion to uncover the complex dynamics of the 2023 Kahramanmaraş, Turkey, Mw 7.8–7.7 earthquake doublet. The Mw 7.8 event consisted of six subevents, occurring over approximately 90 s, and featured three subshear slip episodes. The Mw 7.7 event, which occurred 9 h later, consisted of four major subevents over a total duration of 30 s, with the first three forming a larger slip and a supershear rupture along its western branch.

Apart from that, the CMT inversion has been advanced by considering a better source time function (STF), which is the time derivative of the moment (moment rate function). STF is a crucial source property for depicting the temporal evolution of seismic energy release during an earthquake and has multiple important implications in seismology. The STF reveals details about the earthquake's rupture duration, propagation speed, and heterogeneity (e.g., subevents, slip pulses), helping distinguish between complex and straightforward ruptures (e.g., multi-fault breaks) (e.g., Ruff and Miller, 1994; Ye et al., 2016; Yin et al., 2021). Its time-integration directly yields the scalar moment, a parameter used to estimate the moment magnitude, and also scales with the stress drop, both of which are key parameters for ground motion prediction (Somerville et al., 1999) and hazard assessment (Kanamori and Rivera, 2004). Moreover, STF is an important indicator for identifying tsunami earthquakes and investigating aftershock triggering (Vallée, 2013). Despite its importance, the GCMT catalog does not invert the STF with CMT solutions. Instead, the STF was assumed to be a boxcar before 2004 and recently an isosceles triangle whose duration is empirically determined by the magnitude, as mentioned above. This approximated STF is sufficient for analyzing very long and intermediate-long period waveforms (Fig. 4). At the same time, Stein and Wysession (2003) noted that the imposed relationship between STF duration and magnitude does not hold for short-period bands, and detailed STFs are still required.

Considerable effort has been devoted to determining the STF based on the constrained deconvolution with the STF's physical properties. According to the representation theorem (Aki and Richards, 2002), observed waveforms can be expressed as the temporal convolution of the STF with Green's functions responding to a CMT. Therefore, a straightforward method to retrieve the STF is to deconvolve the observed signals with CMT-generated waveforms. Dreger (1994) used an empirical Green's function (EGF) analysis to retrieve the far-field STF of the 17 January 1994 Northridge (Mw 6.7) earthquake. They identified an Mw 4.4 aftershock with a similar focal mechanism and nearly identical location to the mainshock. They used its waveforms as EGFs by deconvolving them from the mainshock recordings to extract the STF. However, suitable EGFs are not always available for moderate to large earthquakes. As an alternative, Vallée et al. (2011) developed the SCARDEC deconvolution method, which first determines the source depth and focal mechanism through the Neighborhood Algorithm (Sambridge, 1999) and then deconvolves the predicted waveforms from the observed waveforms to obtain the STF.

One of the primary challenges rests in enforcing physical constraints on the retrieved STF. These constraints include causality (the STF must be zero before the origin time), positivity (assuming only forward slip for tectonic earthquakes), and consistency or stability of the seismic moment across all stations (Hirano, 2022; Stähler and Sigloch, 2014). Vallée et al. (2011) proposed an iterative scheme imposing these constraints in their SCADEC deconvolution. Vallée and Douet (2016) used the SCARDEC method to analyze global Mw $>$ 5.8 earthquakes and build a new SCARDEC STF database. The deconvolution approach requires a reliable CMT solution, for which the GCMT catalog has been widely used as a starting point or reference in studies of moderate to large earthquakes.

Another approach is to invert both the STF and the CMT, either iteratively or simultaneously, using short- or long-period waveforms—a highly nonlinear problem. Ruff and Tichelaar (1990) and Šílený et al. (1992) developed an iterative inversion of waveforms with a two-step process: (1) an unconstrained linear inversion to obtain moment tensor rate functions (MTRFs)—five- or six-component time-varying MTs; a constrained non-linear inversion to obtain the representative CMT and a common time-dependency among MTRFs, i.e., STF that best fit all MTRFs. Panza and Sarao (2000) applied this method to data recorded in Italian volcanic regions (Campi Flegrei, Vesuvius, and Mt. Etna) as well as the geothermal area of Larderello. They identified spurious non-double-couple components, which they attributed to poor station coverage, data noise, and inaccuracies in the Earth model. Similarly, Wéber (2009) employed this approach, using waveforms up to 5 Hz, to determine the MTs and STFs for three small local events in Hungary. All three events were dominated by double-couple components, indicating a tectonic origin, and their STFs featured significant energy releases lasting only about 0.1–0.2 s. This method is particularly well-suited for small earthquakes at local scales due to the availability of high-frequency data and a better understanding of the Earth's structures, as well as the validity of the assumption that all stations share a common STF, which holds true for small seismic events.

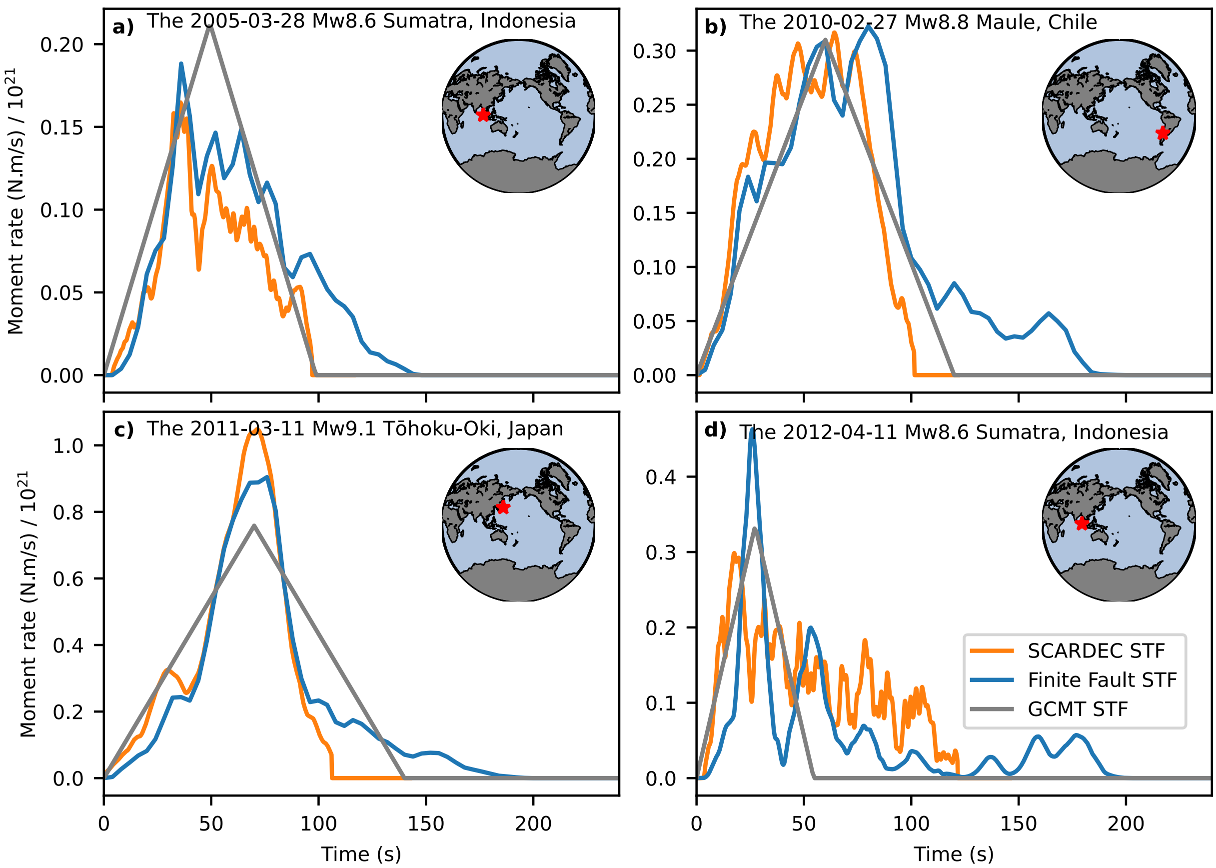

Fig. 4. Source time functions of four notable great earthquakes: (a) the 2005-03-28 Mw8.6 Sumatra earthquake, (b) the 2010-02-27 Mw8.8 Maule earthquake, (c) the 2011-03-11 Mw9.1 Tōhoku-Oki earthquakes, and (d) the 2012-04-11 Mw8.6 Sumatra earthquake. The STFs are compared across three global STF databases: GCMT (green), SCARDEC (orange), and USGS finite fault inversion (blue). (For interpretation of the references to color in this figure legend, the reader is referred to the web version of this article.)

More careful attention is dedicated to treating the assumptions and physical properties of STF for moderate to large earthquakes (Mw $\geq$ 6.0). The assumption that MTRFs have a common time dependency, meaning the focal mechanism does not vary over time, is a feasible consideration for long-period waveforms (Vavryčuk and Kühn, 2012). In a magnitude range of 6.0–7.5, the directivity effect of the source can still be neglected when using body-wave methods (Vallée et al., 2011) so that a common STF can be used by all stations. A widely used approach is to construct the STF as a sum of basis functions, where only its weight factors are determined from the inversion. Stähler and Sigloch (2014) implemented this approach using basis functions determined from Principal Component Analysis (PCA) for a pre-established STF catalog (Sigloch and Nolet, 2006) in a probabilistic inversion because of the reduced dimension of the parameter space. However, for larger earthquakes, the STF varies at stations—apparent STF (ASTF). Xu et al. (2023) developed a three-step method to iteratively invert CMT and ASTF using teleseismic P-wave and W-phase data for large earthquakes.

Despite the advances, determining the STF remains a challenge in seismology. First, the inversion of STF relies on high-frequency waveform modeling due to its higher sensitivity in constraining the variation in the STF (e.g., Wéber, 2009); however, this approach is challenging due to imperfect knowledge of the Earth's structure model (i.e., structural error). Therefore, the effort to build 3D Earth models via seismic tomography would enable the calculation of high-frequency waveforms. Moreover, the uncertainty arising from data noise and structural error should become an integral part of GCMT inference as discussed before. We thus bring this review to a conclusion by recommending that the next-generation catalog include robust CMTs and STFs, including their associated uncertainties.

7. Concluding remarks

This review contributes to the celebration of the paper series published in *Physics of the Earth and Planetary Interior*, focusing on the Ekström et al. (2012) paper, which presented the latest methodological developments on the impactful GCMT project. We reviewed the technical details of the standard and elegant GCMT method and commented on its far-reaching legacy for the Earth science community. Noting that the earthquake location improvement is paramount, we discussed the approaches that could be improved in the future and identified three interconnected research frontiers in the CMT inversion research, with a recommendation for the next generation of the GCMT catalog. These include the improved uncertainty quantification of MT solutions, the utilization of 3D earth structures in MT inversion, and the pursuit of seismic source models that extend beyond the point source assumption in both time and space. Routine joint CMT inversion of multiple adjacent seismic sources will also be a worthwhile research direction. Despite theoretical and practical challenges, recent developments in geophysical inference tools and algorithms, machine learning approaches, and advancements in computational resources will hopefully lead to the integration of one or a combination of these advancements into the next generation of the GCMT earthquake catalog.

CRediT authorship contribution statement

T.-S. Phạm: Writing – review & editing, Writing – original draft, Visualization, Investigation, Funding acquisition, Conceptualization. **H. Tkalčić:** Writing – review & editing, Writing – original draft, Investigation, Funding acquisition, Conceptualization. **J. Hu:** Writing – review

& editing, Writing – original draft, Visualization, Investigation, Conceptualization. **Z. Wei:** Writing – review & editing, Writing – original draft, Visualization, Investigation, Conceptualization.

Declaration of competing interest

The authors declare the following financial interests/personal relationships which may be considered as potential competing interests:

Thanh-Son Pham reports financial support was provided by Australian Research Council. Hrvoje Tkalcic reports financial support was provided by Australian Research Council. Hrvoje Tkalcic reports financial support was provided by Air Force Research Laboratory. If there are other authors, they declare that they have no known competing financial interests or personal relationships that could have appeared to influence the work reported in this paper.

Acknowledgments

We are grateful to the editor Ana Ferreira for her kind invitation to contribute to this special issue. We thank Göran Ekström and an anonymous reviewer for their thoughtful comments that improved the quality of the final manuscript. T.-S. P. and H. T. acknowledge financial support from the Australian Research Council through a Discovery Early Career Research Award (DE230100025) and a Discovery Proposal (DP140102533). Additionally, H. T. is grateful for continuing support for seismic source studies through the US DoD/DoE and AFRL competitive Broad Agency Announcement schemes. We acknowledge computational support by the National Computational Infrastructure.

Data availability

The GCMT catalog was accessed at www.globalcmt.org.

References

Aki, K., Richards, P.G., 2002. Quantitative Seismology, Second ed. University Science Books, Sausalito, CA.
Albuquerque Seismological Laboratory (ASL)/USGS, 1992. New China Digital Seismograph Network. https://doi.org/10.7914/SN/IC.
Albuquerque Seismological Laboratory (ASL)/USGS, 1993. Global Telemetered Seismograph Network (USAF/USGS). https://doi.org/10.7914/SN/GT.
Albuquerque Seismological Laboratory (ASL)/USGS, 2006. Caribbean Network. https://doi.org/10.7914/SN/CU.
Albuquerque Seismological Laboratory/USGS, 1988. Global Seismograph Network (GSN - IRIS/USGS). https://doi.org/10.7914/SN/IU.
Alsing, J., Wandelt, B., 2019. Nuisance hardened data compression for fast likelihood-free inference. Mon. Not. R. Astron. Soc. 488, 5093–5103. https://doi.org/10.1093/mnras/stz1900.
Altamimi, Z., Rebischung, P., Métivier, L., Collilieux, X., 2016. ITRF2014: a new release of the International Terrestrial Reference Frame modeling nonlinear station motions. J. Geophys. Res. Solid Earth 121, 6109–6131. https://doi.org/10.1002/2016JB013098.
Alvizuri, C., Tape, C., 2018. Full moment tensor analysis of nuclear explosions in North Korea. Seismol. Res. Lett. 89, 2139–2151. https://doi.org/10.1785/0220180158.
Ammon, C.J., Ji, C., Thio, H.-K., Robinson, D., Ni, S., Hjorleifsdottir, V., Kanamori, H., Lay, T., Das, S., Helmberger, D., Ichinose, G., Polet, J., Wald, D., 2005. Rupture process of the 2004 Sumatra-Andaman earthquake. Science 308, 1133–1139. https://doi.org/10.1126/science.1112260.
Arvidsson, R., Ekström, G., 1998. Global CMT analysis of moderate earthquakes, $mw \geqq 4.5$, using intermediate-period surface waves. Bull. Seismol. Soc. Am. 88, 1003–1013. https://doi.org/10.1785/BSSA0880041003.
Aster, R.C., Borchers, B., Thurber, C.H., 2013. Bayesian methods. In: Parameter Estimation and Inverse Problems. Elsevier, pp. 253–280. https://doi.org/10.1016/B978-0-12-385048-5.00011-2.
Banerdt, W.B., Smrekar, S.E., Banfield, D., Giardini, D., Golombek, M., Johnson, C.L., Lognonné, P., Spiga, A., Spohn, T., Perrin, C., Stähler, S.C., Antonangeli, D., Asmar, S., Beghein, C., Bowles, N., Bozdag, E., Chi, P., Christensen, U., Clinton, J., Collins, G.S., Daubar, I., Dehant, V., Drilleau, M., Fillingim, M., Folkner, W., Garcia, R.F., Garvin, J., Grant, J., Grott, M., Grygorczuk, J., Hudson, T., Irving, J.C. E., Kargl, G., Kawamura, T., Kedar, S., King, S., Knapmeyer-Endrun, B., Knapmeyer, M., Lemmon, M., Lorenz, R., Maki, J.N., Margerin, L., McLennan, S.M., Michaut, C., Mimoun, D., Mittelholz, A., Mocquet, A., Morgan, P., Mueller, N.T., Murdoch, N., Nagihara, S., Newman, C., Nimmo, F., Panning, M., Pike, W.T., Plesa, A.-C., Rodriguez, S., Rodriguez-Manfredi, J.A., Russell, C.T., Schmerr, N., Siegler, M., Stanley, S., Stutzmann, E., Teanby, N., Tromp, J., van Driel, M., Warner, N., Weber, R., Wieczorek, M., 2020. Initial results from the InSight mission on Mars. Nat. Geosci. 13, 183–189. https://doi.org/10.1038/s41561-020-0544-y.
Baxter, A.T., Hannington, M.D., Stewart, M.S., Emberley, J.M., Breker, K., Krätschell, A., Petersen, S., Brandl, P.A., Klischies, M., Mensing, R., Anderson, M.O., 2020. Shallow seismicity and the classification of structures in the Lau Back-Arc Basin. Geochem. Geophys. Geosyst. 21, e2020GC008924. https://doi.org/10.1029/2020GC008924.
Bayona, J.A., Savran, W., Strader, A., Hainzl, S., Cotton, F., Schorlemmer, D., 2021. Two global ensemble seismicity models obtained from the combination of interseismic strain measurements and earthquake-catalogue information. Geophys. J. Int. 224, 1945–1955. https://doi.org/10.1093/gji/ggaa554.
Betancourt, M., 2018. A Conceptual Introduction to Hamiltonian Monte Carlo. (ArXiv170102434 Stat).
Bird, P., Jackson, D.D., Kagan, Y.Y., Kreemer, C., Stein, R.S., 2015. GEAR1: a global earthquake activity rate model constructed from geodetic strain rates and smoothed seismicity. Bull. Seismol. Soc. Am. 105, 2538–2554. https://doi.org/10.1785/0120150058.
Blom, N., Hardalupas, P.-S., Rawlinson, N., 2023. Mitigating the effect of errors in source parameters on seismic (waveform) tomography. Geophys. J. Int. 232, 810–828. https://doi.org/10.1093/gji/ggac314.
Bozdağ, E., Peter, D., Lefebvre, M., Komatitsch, D., Tromp, J., Hill, J., Podhorszki, N., Pugmire, D., 2016. Global adjoint tomography: first-generation model. Geophys. J. Int. 207, 1739–1766. https://doi.org/10.1093/gji/ggw356.
California Institute of Technology and United States Geological Survey Pasadena, 1926. Southern California Seismic Network. https://doi.org/10.7914/SN/CI.
Chiang, A., Dreger, D.S., Ford, S.R., Walter, W.R., 2014. Source characterization of underground explosions from combined regional moment tensor and first-motion analysis. Bull. Seismol. Soc. Am. 104, 1587–1600. https://doi.org/10.1785/0120130228.
Chiang, A., Ford, S.R., Pasyanos, M.E., Simmons, N.A., 2025. Bayesian inference for the seismic moment tensor using regional waveforms and Teleseismic-P polarities with a data-derived distribution of velocity models and source locations. Bull. Seismol. Soc. Am. https://doi.org/10.1785/0120240226.
Clévédé, E., Bouin, M.-P., Bukchin, B., Mostinskiy, A., Patau, G., 2004. New constraints on the rupture process of the 1999 august 17 Izmit earthquake deduced from estimates of stress glut rate moments. Geophys. J. Int. 159, 931–942. https://doi.org/10.1111/j.1365-246X.2004.02304.x.
Dahlen, F.A., Tromp, J., 1998. Theoretical global seismology. In: Princton, N.J. Princeton University Press.
Dapré, K., Irving, J.C.E., 2025. Seismic wavefield modeling of Enceladus: challenges and opportunities presented by a 3D ice shell. J. Geophys. Res. Planets 130, e2024JE008644. https://doi.org/10.1029/2024JE008644.
Del Moral, P., Doucet, A., Jasra, A., 2006. Sequential Monte Carlo samplers. J. R. Stat. Soc. B 68, 411–436.
Dettmer, J., Dosso, S.E., 2012. Trans-dimensional matched-field geoacoustic inversion with hierarchical error models and interacting Markov chains. J. Acoust. Soc. Am. 132, 2239–2250. https://doi.org/10.1121/1.4746016.
Dinh, L., Sohl-Dickstein, J., Bengio, S., 2016. Density Estimation Using Real NVP. https://doi.org/10.48550/ARXIV.1605.08803.
Donner, S., Mustać, M., Hejrani, B., Tkalčić, H., Igel, H., 2020. Seismic moment tensors from synthetic rotational and translational ground motion: Green's functions in 1-D versus 3-D. Geophys. J. Int. 223 (1), 161–179. https://doi.org/10.1093/gji/ggaa305.
Dreger, D.S., 1994. Empirical green's function study of the January 17, 1994 Northridge, California earthquake. Geophys. Res. Lett. 21, 2633–2636. https://doi.org/10.1029/94GL02661.
Dreger, D.S., Gritto, R., Nelson, O., 2021. Path calibration of the Democratic People's Republic of Korea 3 September 2017 nuclear test. Seismol. Res. Lett. 92, 3375–3385. https://doi.org/10.1785/0220210105.
Duputel, Z., Rivera, L., Fukahata, Y., Kanamori, H., 2012. Uncertainty estimations for seismic source inversions. Geophys. J. Int. 190, 1243–1256. https://doi.org/10.1111/j.1365-246X.2012.05554.x.
Dziewoński, A.M., Anderson, D.L., 1981. Preliminary reference earth model. Phys. Earth Planet. Inter. 25, 297–356. https://doi.org/10.1016/0031-9201(81)90046-7.
Dziewoński, A.M., Woodhouse, J.H., 1983. An experiment in systematic study of global seismicity: centroid-moment tensor solutions for 201 moderate and large earthquakes of 1981. J. Geophys. Res. Solid Earth 88, 3247–3271. https://doi.org/10.1029/JB088iB04p03247.
Dziewoński, A.M., Woodward, R.L., 1992. Acoustic imaging at the planetary scale. In: Ermert, H., Harjes, H.-P. (Eds.), Acoustical Imaging. Springer US, Boston, MA, pp. 785–797. https://doi.org/10.1007/978-1-4615-3370-2_124.
Dziewoński, A.M., Chou, T.-A., Woodhouse, J.H., 1981. Determination of earthquake source parameters from waveform data for studies of global and regional seismicity. J. Geophys. Res. Solid Earth 86, 2825–2852. https://doi.org/10.1029/JB086iB04p02825.
EarthScope Consortium, 1986. Global Seismograph Network - II. https://doi.org/10.7914/SN/II.
Eisner, L., Clayton, R.W., 2001. A reciprocity method for multiple-source simulations. Bull. Seismol. Soc. Am. 91, 553–560. https://doi.org/10.1785/0120000222.
Ekström, G., 2006. Global detection and location of seismic sources by using surface waves. Bull. Seismol. Soc. Am. 96, 1201–1212. https://doi.org/10.1785/0120050175.
Ekström, G., 2007. 4.16 - global seismicity: Results from systematic waveform analyses, 1976–2005. In: Schubert, G. (Ed.), Treatise on Geophysics. Elsevier, Amsterdam, pp. 473–481. https://doi.org/10.1016/B978-044452748-6.00077-8.

Ekström, G., 2011. A global model of love and Rayleigh surface wave dispersion and anisotropy, 25-250 s: global dispersion model GDM52. Geophys. J. Int. 187, 1668–1686. https://doi.org/10.1111/j.1365-246X.2011.05225.x.

Ekström, G., Tromp, J., Larson, E.W.F., 1997. Measurements and global models of surface wave propagation. J. Geophys. Res. Solid Earth 102, 8137–8157. https://doi.org/10.1029/96JB03729.

Ekström, G., Morelli, A., Boschi, E., Dziewoński, A.M., 1998. Moment tensor analysis of the Central Italy earthquake sequence of September–October 1997. Geophys. Res. Lett. 25, 1971–1974. https://doi.org/10.1029/98GL01241.

Ekström, G., Nettles, M., Abers, G.A., 2003. Glacial earthquakes. Science 302, 622–624. https://doi.org/10.1126/science.1088057.

Ekström, G., Nettles, M., Dziewoński, A.M., 2012. The global CMT project 2004–2010: centroid-moment tensors for 13,017 earthquakes. Phys. Earth Planet. Inter. 200–201, 1–9. https://doi.org/10.1016/j.pepi.2012.04.002.

Elliott, J.R., Jolivet, R., González, P.J., Avouac, J.-P., Hollingsworth, J., Searle, M.P., Stevens, V.L., 2016a. Himalayan megathrust geometry and relation to topography revealed by the Gorkha earthquake. Nat. Geosci. 9, 174–180. https://doi.org/10.1038/ngeo2623.

Elliott, J.R., Walters, R.J., Wright, T.J., 2016b. The role of space-based observation in understanding and responding to active tectonics and earthquakes. Nat. Commun. 7, 13844. https://doi.org/10.1038/ncomms13844.

Engdahl, E.R., Di Giacomo, D., Sakarya, B., Gkarlaouni, C.G., Harris, J., Storchak, D.A., 2020. ISC-EHB 1964–2016, an improved data set for studies of earth structure and global seismicity. Earth Space Sci. 7, e2019EA000897. https://doi.org/10.1029/2019EA000897.

Ferreira, A.M.G., Woodhouse, J.H., 2006. Long-period seismic source inversions using global tomographic models. Geophys. J. Int. 166, 1178–1192. https://doi.org/10.1111/j.1365-246X.2006.03003.x.

Ferreira, A.M.G., Woodhouse, J.H., 2007. Source, path and receiver effects on seismic surface waves. Geophys. J. Int. 168, 109–132. https://doi.org/10.1111/j.1365-246X.2006.03092.x.

Fichtner, A., Simutė, S., 2018. Hamiltonian Monte Carlo inversion of seismic sources in complex media. J. Geophys. Res. Solid Earth 123, 2984–2999. https://doi.org/10.1002/2017JB015249.

Fichtner, A., Kennett, B.L.N., Igel, H., Bunge, H.-P., 2009. Full seismic waveform tomography for upper-mantle structure in the Australasian region using adjoint methods. Geophys. J. Int. 179, 1703–1725. https://doi.org/10.1111/j.1365-246X.2009.04368.x.

Fichtner, A., Kennett, B.L.N., Igel, H., Bunge, H.-P., 2010. Full waveform tomography for radially anisotropic structure: new insights into present and past states of the Australasian upper mantle. Earth Planet. Sci. Lett. 290, 270–280. https://doi.org/10.1016/j.epsl.2009.12.003.

Fishwick, S., Rawlinson, N., 2012. 3-D structure of the Australian lithosphere from evolving seismic datasets. Aust. J. Earth Sci. 59, 809–826. https://doi.org/10.1080/08120099.2012.702319.

Ford, S.R., Dreger, D.S., Walter, W.R., 2010. Network sensitivity solutions for regional moment-tensor inversions network sensitivity solutions for regional moment-tensor inversions. Bull. Seismol. Soc. Am. 100, 1962–1970. https://doi.org/10.1785/0120090140.

Ford, S.R., Walter, W.R., Dreger, D.S., 2012. Event discrimination using regional moment tensors with Teleseismic-P constraints. Bull. Seismol. Soc. Am. 102, 867–872. https://doi.org/10.1785/0120110227.

Frohlich, C., Davis, S.D., 1999. How well constrained are well-constrained T, B, and P axes in moment tensor catalogs? J. Geophys. Res. Solid Earth 104, 4901–4910. https://doi.org/10.1029/1998JB900071.

Geological Survey, U.S., 2017. The Preliminary Determination of Epicenters (PDE) Bulletin. https://doi.org/10.5066/F74T6GJC.

Gilbert, F., 1971. Excitation of the normal modes of the earth by earthquake sources. Geophys. J. Int. 22, 223–226. https://doi.org/10.1111/j.1365-246X.1971.tb03593.x.

Gokhberg, A., Fichtner, A., 2016. Full-waveform inversion on heterogeneous HPC systems. Comput. Geosci. 89, 260–268. https://doi.org/10.1016/j.cageo.2015.12.013.

Goodman, J., Weare, J., 2010. Ensemble samplers with affine invariance. Commun. Appl. Math. Comput. Sci. 5, 65–80. https://doi.org/10.2140/camcos.2010.5.65.

Gualtieri, L., Ekström, G., 2018. Broad-band seismic analysis and modeling of the 2015 Taan Fjord, Alaska landslide using Instaseis. Geophys. J. Int. 213, 1912–1923. https://doi.org/10.1093/gji/ggy086.

Hallo, M., Gallovič, F., 2016. Fast and cheap approximation of green function uncertainty for waveform-based earthquake source inversions. Geophys. J. Int. 207, 1012–1029. https://doi.org/10.1093/gji/ggw320.

Hayes, G.P., Moore, G.L., Portner, D.E., Hearne, M., Flamme, H., Furtney, M., Smoczyk, G.M., 2018. Slab2, a comprehensive subduction zone geometry model. Science 362, 58–61. https://doi.org/10.1126/science.aat4723.

Hejrani, B., Tkalčić, H., 2020. Resolvability of the centroid-moment-tensors for shallow seismic sources and improvements from modeling high-frequency waveforms. J. Geophys. Res. Solid Earth 125, e2020JB019643. https://doi.org/10.1029/2020JB019643.

Hejrani, B., Tkalčić, H., Fichtner, A., 2017. Centroid moment tensor catalogue using a 3-D continental scale earth model: application to earthquakes in Papua New Guinea and the Solomon Islands. J. Geophys. Res. Solid Earth 122, 5517–5543. https://doi.org/10.1002/2017JB014230.

Helffrich, G.R., 1997. How good are routinely determined focal mechanisms? Empirical statistics based on a comparison of Harvard, USGS and ERI moment tensors. Geophys. J. Int. 131, 741–750. https://doi.org/10.1111/j.1365-246X.1997.tb06609.x.

Hingee, M., Tkalčić, H., Fichtner, A., Sambridge, M., 2011. Seismic moment tensor inversion using a 3-D structural model: applications for the Australian region: moment tensor inversion using 3-D earth. Geophys. J. Int. 184, 949–964. https://doi.org/10.1111/j.1365-246X.2010.04897.x.

Hirano, S., 2022. Source time functions of earthquakes based on a stochastic differential equation. Sci. Rep. 12, 3936. https://doi.org/10.1038/s41598-022-07873-2.

Hjörleifsdóttir, V., Ekström, G., 2010. Effects of three-dimensional earth structure on CMT earthquake parameters. Phys. Earth Planet. Inter. 179, 178–190. https://doi.org/10.1016/j.pepi.2009.11.003.

Hu, J., Phạm, T.-S., Tkalčić, H., 2023. Seismic moment tensor inversion with theory errors from 2-D earth structure: implications for the 2009–2017 DPRK nuclear blasts. Geophys. J. Int. 235, 2035–2054. https://doi.org/10.1093/gji/ggad348.

Hu, J., Phạm, T.-S., Tkalčić, H., 2024. A composite seismic source model for the first major event during the 2022 Hunga (Tonga) volcanic eruption. Geophys. Res. Lett. 51, e2024GL109442. https://doi.org/10.1029/2024GL109442.

Jia, Z., Shen, Z., Zhan, Z., Li, C., Peng, Z., Gurnis, M., 2020. The 2018 Fiji M 8.2 and 7.9 deep earthquakes: one doublet in two slabs. Earth Planet. Sci. Lett. 531, 115997. https://doi.org/10.1016/j.epsl.2019.115997.

Jia, Z., Zhan, Z., Kanamori, H., 2022. The 2021 South Sandwich Island M_w 8.2 earthquake: a slow event sandwiched between regular ruptures. Geophys. Res. Lett. 49, e2021GL097104. https://doi.org/10.1029/2021GL097104.

Jia, Z., Jin, Z., Marchandon, M., Ulrich, T., Gabriel, A.-A., Fan, W., Shearer, P., Zou, X., Rekoske, J., Bulut, F., Garagon, A., Fialko, Y., 2023. The complex dynamics of the 2023 Kahramanmaraş, Turkey, M_w 7.8-7.7 earthquake doublet. Science 381, 985–990. https://doi.org/10.1126/science.adi0685.

Jost, M.L., Herrmann, R.B., 1989. A student's guide to and review of moment tensors. Seismol. Res. Lett. 60, 37–57. https://doi.org/10.1785/gssrl.60.2.37.

Julian, B.R., 1986. Analysing seismic-source mechanisms by linear-programming methods. Geophys. J. Int. 84, 431–443. https://doi.org/10.1111/j.1365-246X.1986.tb04364.x.

Julian, B.R., Miller, A.D., Foulger, G.R., 1998. Non-double-couple earthquakes 1. Theory. Rev. Geophys. 36, 525–549. https://doi.org/10.1029/98RG00716.

Kanamori, H., Given, J.W., 1982. Analysis of long-period seismic waves excited by the may 18, 1980, eruption of Mount St. Helens—a terrestrial monopole? J. Geophys. Res. Solid Earth 87, 5422–5432. https://doi.org/10.1029/JB087iB07p05422.

Kanamori, H., Rivera, L., 2004. Static and dynamic scaling relations for earthquakes and their implications for rupture speed and stress drop. Bull. Seismol. Soc. Am. 94, 314–319. https://doi.org/10.1785/0120030159.

Kawakatsu, H., 1989. Centroid single force inversion of seismic waves generated by landslides. J. Geophys. Res. Solid Earth 94, 12363–12374. https://doi.org/10.1029/JB094iB09p12363.

Kawakatsu, H., 1996. Observability of the isotropic component of a moment tensor. Geophys. J. Int. 126, 525–544. https://doi.org/10.1111/j.1365-246X.1996.tb05308.x.

Kawakatsu, H., 2024. Characterizing lithospheric transverse isotropy using moment tensors—on the origin of the non–double-couple components of global CMT solutions. Bull. Seismol. Soc. Am. 114, 2995–3010. https://doi.org/10.1785/0120240136.

Kim, Y., Liu, Q., Tromp, J., 2011. Adjoint centroid-moment tensor inversions: Adjoint centroid-moment tensor inversions. Geophys. J. Int. 186, 264–278. https://doi.org/10.1111/j.1365-246X.2011.05027.x.

Kim, S., Tkalčić, H., Rhie, J., Chen, Y., 2016. Intraplate volcanism controlled by back-arc and continental structures in NE Asia inferred from transdimensional Bayesian ambient noise tomography. Geophys. Res. Lett. 43, 8390–8398. https://doi.org/10.1002/2016GL069483.

Komatitsch, D., Tromp, J., 1999. Introduction to the spectral element method for three-dimensional seismic wave propagation. Geophys. J. Int. 139, 806–822. https://doi.org/10.1046/j.1365-246x.1999.00967.x.

Komatitsch, D., Tromp, J., 2002a. Spectral-element simulations of global seismic wave propagation—II. Three-dimensional models, oceans, rotation and self-gravitation. Geophys. J. Int. 150, 303–318. https://doi.org/10.1046/j.1365-246X.2002.01716.x.

Komatitsch, D., Tromp, J., 2002b. Spectral-element simulations of global seismic wave propagation—I. Validation. Geophys. J. Int. 149, 390–412. https://doi.org/10.1046/j.1365-246X.2002.01653.x.

Kustowski, B., Ekström, G., Dziewoński, A.M., 2008. Anisotropic shear-wave velocity structure of the Earth's mantle: a global model. J. Geophys. Res. Solid Earth 113, 2007JB005169. https://doi.org/10.1029/2007JB005169.

Lee, E.-J., Chen, P., Jordan, T.H., Wang, L., 2011. Rapid full-wave centroid moment tensor (CMT) inversion in a three-dimensional earth structure model for earthquakes in Southern California. Geophys. J. Int. 186, 311–330. https://doi.org/10.1111/j.1365-246X.2011.05031.x.

Lee, E.J., Chen, P., Jordan, T.H., Wang, L., 2011. Rapid full-wave centroid moment tensor (CMT) inversion in a three-dimensional earth structure model for earthquakes in Southern California. Geophys. J. Int. 186 (1), 311–330.

Lei, W., Ruan, Y., Bozdağ, E., Peter, D., Lefebvre, M., Komatitsch, D., Tromp, J., Hill, J., Podhorszki, N., Pugmire, D., 2020. Global adjoint tomography—model GLAD-M25. Geophys. J. Int. 223, 1–21. https://doi.org/10.1093/gji/ggaa253.

Lentas, K., 2018. Towards routine determination of focal mechanisms obtained from first motion P-wave arrivals. Geophys. J. Int. 212, 1665–1686. https://doi.org/10.1093/gji/ggx503.

Lentas, K., Di Giacomo, D., Harris, J., Storchak, D.A., 2019. The ISC bulletin as a comprehensive source of earthquake source mechanisms. Earth Syst. Sci. Data 11, 565–578. https://doi.org/10.5194/essd-11-565-2019.

Li, Y., Gurnis, M., 2024. Rapid shear zone weakening during subduction initiation. Proc. Natl. Acad. Sci. 121, e2404939121. https://doi.org/10.1073/pnas.2404939121.

Liu, Q., 2004. Spectral-element moment tensor inversions for earthquakes in Southern California. Bull. Seismol. Soc. Am. 94, 1748–1761. https://doi.org/10.1785/012004038.

Lloyd, A.J., Wiens, D.A., Zhu, H., Tromp, J., Nyblade, A.A., Aster, R.C., Hansen, S.E., Dalziel, I.W.D., Wilson, T.J., Ivins, E.R., O'Donnell, J.P., 2020. Seismic structure of the Antarctic upper mantle imaged with adjoint tomography. J. Geophys. Res. Solid Earth 125. https://doi.org/10.1029/2019JB017823.

Ma, Z., Masters, G., 2015. Effect of earthquake locations on Rayleigh wave azimuthal anisotropy models. Geophys. J. Int. 203, 1319–1333. https://doi.org/10.1093/gji/ggv369.

Maeda, T., Takemura, S., Furumura, T., 2017. OpenSWPC: an open-source integrated parallel simulation code for modeling seismic wave propagation in 3D heterogeneous viscoelastic media. Earth Planets Space 69, 102. https://doi.org/10.1186/s40623-017-0687-2.

McGuire, J.J., Zhao, L., Jordan, T.H., 2001. Teleseismic inversion for the second-degree moments of earthquake space-time distributions. Geophys. J. Int. 145, 661–678. https://doi.org/10.1046/j.1365-246x.2001.01414.x.

Métivier, L., Collilieux, X., Lercier, D., Altamimi, Z., Beauducel, F., 2014. Global coseismic deformations, GNSS time series analysis, and earthquake scaling laws. J. Geophys. Res. Solid Earth 119, 9095–9109. https://doi.org/10.1002/2014JB011280.

Mustać, M., Tkalčić, H., 2016. Point source moment tensor inversion through a Bayesian hierarchical model. Geophys. J. Int. 204, 311–323. https://doi.org/10.1093/gji/ggv458.

Mustać, M., Tkalčić, H., Burky, A.L., 2018. The variability and interpretation of earthquake source mechanisms in the geysers geothermal field from a Bayesian standpoint based on the choice of a noise model. J. Geophys. Res. Solid Earth 123, 2017JB014897. https://doi.org/10.1002/2017JB014897.

Mustać, M., Hejrani, B., Tkalčić, H., Kim, S., Lee, S.-J., Cho, C.-S., 2020. Large isotropic component in the source mechanism of the 2013 Democratic People's Republic of Korea nuclear test revealed via a hierarchical Bayesian inversion. Bull. Seismol. Soc. Am. 110, 166–177. https://doi.org/10.1785/0120190062.

Nakano, M., Yamashina, T., Kumagai, H., Inoue, H., Sunarjo, 2010. Centroid moment tensor catalogue for Indonesia. Phys. Earth Planet. Inter. 183, 456–467. https://doi.org/10.1016/j.pepi.2010.10.010.

Nettles, M., Ekström, G., 2010. Glacial earthquakes in Greenland and Antarctica. Annu. Rev. Earth Planet. Sci. 38, 467–491. https://doi.org/10.1146/annurev-earth-040809-152414.

Northern California Earthquake Data Center, 2014. Berkeley Digital Seismic Network (BDSN). https://doi.org/10.7932/BDSN.

Olive, J.-A., Ekström, G., Buck, W.R., Liu, Z., Escartín, J., Bickert, M., 2024. Mid-ocean ridge unfaulting revealed by magmatic intrusions. Nature 628, 782–787. https://doi.org/10.1038/s41586-024-07247-w.

Olsen, K.G., Nettles, M., 2017. Patterns in glacial-earthquake activity around Greenland, 2011–13. J. Glaciol. 63, 1077–1089. https://doi.org/10.1017/jog.2017.78.

Panza, G.F., Sarao, A., 2000. Monitoring volcanic and geothermal areas by full seismic moment tensor inversion: are non-double-couple components always artefacts of modelling? Geophys. J. Int. 143, 353–364. https://doi.org/10.1046/j.1365-246X.2000.01250.x.

Papamakarios, G., Pavlakou, T., Murray, I., 2017. Masked autoregressive flow for density estimation. In: Advances in Neural Information Processing Systems. Curran Associates, Inc.

Phạm, T.-S., 2024. Gradient-based joint inversion of point-source moment tensor and station-specific time-shifts. Geophys. J. Int. 238, 783–793. https://doi.org/10.1093/gji/ggae188.

Phạm, T.-S., Tkalčić, H., 2021. Toward improving point-source moment-tensor inference by incorporating 1D earth model's uncertainty: implications for the Long Valley Caldera Earthquakes. J. Geophys. Res. Solid Earth 126, 2021JB022477. https://doi.org/10.1029/2021JB022477.

Phạm, T.-S., Tkalčić, H., Hu, J., Kim, S., 2024. Towards a new standard for seismic moment tensor inversion containing 3-D earth structure uncertainty. Geophys. J. Int. 238, 1840–1853. https://doi.org/10.1093/gji/ggae256.

Poppeliers, C., Preston, L., 2020. The effects of earth model uncertainty on the inversion of seismic data for seismic source functions. Geophys. J. Int. 224, 100–120. https://doi.org/10.1093/gji/ggaa408.

Rasht-Behesht, M., Huber, C., Shukla, K., Karniadakis, G.E., 2022. Physics-informed neural networks (PINNs) for wave propagation and full waveform inversions. J. Geophys. Res. Solid Earth 127, e2021JB023120. https://doi.org/10.1029/2021JB023120.

Ritsema, J., Heijst, H.J.V., Woodhouse, J.H., 1999. Complex shear wave velocity structure imaged beneath Africa and Iceland. Science 286, 1925–1928. https://doi.org/10.1126/science.286.5446.1925.

Roberts, G.O., Rosenthal, J.S., 2001. Optimal scaling for various metropolis-hastings algorithms. Stat. Sci. 16, 351–367.

Rösler, B., Stein, S., 2022. Consistency of non-double-couple components of seismic moment tensors with earthquake magnitude and mechanism. Seismol. Res. Lett. 93, 1510–1523. https://doi.org/10.1785/0220210188.

Rösler, B., Stein, S., Spencer, B.D., 2021. Uncertainties in seismic moment tensors inferred from differences between global catalogs. Seismol. Res. Lett. 92, 3698–3711. https://doi.org/10.1785/0220210066.

Rösler, B., Spencer, B.D., Stein, S., 2024a. Which global moment tensor catalog provides the most precise non-double-couple components? Seismol. Res. Lett. 95, 2444–2451. https://doi.org/10.1785/0220230372.

Rösler, B., Stein, S., Ringler, A., Vackář, J., 2024b. Apparent non-double-couple components as artifacts of moment tensor inversion. Seismica 3. https://doi.org/10.26443/seismica.v3i1.1157.

Ruff, L.J., Miller, A.D., 1994. Rupture process of large earthquakes in the northern Mexico subduction zone. Pure Appl. Geophys. 142, 101–172. https://doi.org/10.1007/BF00875970.

Ruff, L.J., Tichelaar, B.W., 1990. Moment tensor rate functions for the 1989 Loma Prieta earthquake. Geophys. Res. Lett. 17, 1187–1190. https://doi.org/10.1029/GL017i008p01187.

Sambridge, M., 1999. Geophysical inversion with a neighbourhood algorithm—I. Searching a parameter space. Geophys. J. Int. 138, 479–494. https://doi.org/10.1046/j.1365-246X.1999.00876.x.

Saoulis, A.A., Piras, D., Spurio Mancini, A., Joachimi, B., Ferreira, A.M.G., 2025. Full-waveform earthquake source inversion using simulation-based inference. Geophys. J. Int. 241, 1740–1761. https://doi.org/10.1093/gji/ggaf112.

Sawade, L., Beller, S., Lei, W., Tromp, J., 2022. Global centroid moment tensor solutions in a heterogeneous earth: the CMT3D catalogue. Geophys. J. Int. 231, 1727–1738. https://doi.org/10.1093/gji/ggac280.

Sawade, L., Ekström, G., Ding, L., Nettles, M., Tromp, J., 2025. Parsimonious green function data bases for global centroid moment tensor inversions. Geophys. J. Int. 240, 1986–1999. https://doi.org/10.1093/gji/ggae446.

Schaeffer, A.J., Lebedev, S., 2013. Global shear speed structure of the upper mantle and transition zone. Geophys. J. Int. 194, 417–449. https://doi.org/10.1093/gji/ggt095.

Scheiter, M., Valentine, A., Sambridge, M., 2022. Upscaling and downscaling Monte Carlo ensembles with generative models. Geophys. J. Int. 230, 916–931. https://doi.org/10.1093/gji/ggac100.

Shapiro, N.M., Campillo, M., Stehly, L., Ritzwoller, M.H., 2005. High-resolution surface-wave tomography from ambient seismic noise. Science 307, 1615–1618. https://doi.org/10.1126/science.1108339.

Sigloch, K., Nolet, G., 2006. Measuring finite-frequency body-wave amplitudes and traveltimes. Geophys. J. Int. 167, 271–287. https://doi.org/10.1111/j.1365-246X.2006.03116.x.

Šílený, J., Panza, G.F., Campus, P., 1992. Waveform inversion for point source moment tensor retrieval with variable hypocentral depth and structural model. Geophys. J. Int. 109, 259–274. https://doi.org/10.1111/j.1365-246X.1992.tb00097.x.

Simutė, S., Steptoe, H., Cobden, L., Gokhberg, A., Fichtner, A., 2016. Full-waveform inversion of the Japanese Islands region. J. Geophys. Res. Solid Earth 121, 3722–3741. https://doi.org/10.1002/2016JB012802.

Simutė, S., Boehm, C., Krischer, L., Gokhberg, A., Vallée, M., Fichtner, A., 2023. Bayesian seismic source inversion with a 3-D earth model of the Japanese Islands. J. Geophys. Res. Solid Earth 128, e2022JB024231. https://doi.org/10.1029/2022JB024231.

Sjögreen, B., Petersson, N.A., 2012. A fourth order accurate finite difference scheme for the elastic wave equation in second order formulation. J. Sci. Comput. 52, 17–48. https://doi.org/10.1007/s10915-011-9531-1.

Somerville, P., Irikura, K., Graves, R., Sawada, S., Wald, D., Abrahamson, N., Iwasaki, Y., Kagawa, T., Smith, N., Kowada, A., 1999. Characterizing crustal earthquake slip models for the prediction of strong ground motion. Seismol. Res. Lett. 70, 59–80. https://doi.org/10.1785/gssrl.70.1.59.

Stähler, S.C., Sigloch, K., 2014. Fully probabilistic seismic source inversion - part 1: efficient parameterisation. Solid Earth 5, 1055–1069. https://doi.org/10.5194/se-5-1055-2014.

Stein, S., Wysession, M., 2003. An Introduction to Seismology, Earthquakes, and Earth Structure, 1, edition. ed. Blackwell Publishing, Malden, MA.

Stump, B.W., Johnson, L.R., 1982. Higher-degree moment tensors — the importance of source finiteness and rupture propagation on seismograms. Geophys. J. Int. 69, 721–743. https://doi.org/10.1111/j.1365-246X.1982.tb02772.x.

Süss, M.P., Shaw, J.H., 2003. *P* wave seismic velocity structure derived from sonic logs and industry reflection data in the Los Angeles basin, California. J. Geophys. Res. Solid Earth 108, 2001JB001628. https://doi.org/10.1029/2001JB001628.

Svennevig, K., Hicks, S.P., Forbriger, T., Lecocq, T., Widmer-Schnidrig, R., Mangeney, A., Hibert, C., Korsgaard, N.J., Lucas, A., Satriano, C., Anthony, R.E., Mordret, A., Schippkus, S., Rysgaard, S., Boone, W., Gibbons, S.J., Cook, K.L., Glimsdal, S., Løvholt, F., Van Noten, K., Assink, J.D., Marboeuf, A., Lomax, A., Vanneste, K., Taira, T., Spagnolo, M., De Plaen, R., Koelemeijer, P., Ebeling, C., Cannata, A., Harcourt, W.D., Cornwell, D.G., Caudron, C., Poli, P., Bernard, P., Larose, E., Stutzmann, E., Voss, P.H., Lund, B., Cannavo, F., Castro-Díaz, M.J., Chaves, E., Dahl-Jensen, T., Pinho Dias, N.D., Déprez, A., Develter, R., Dreger, D., Evers, L.G., Fernández-Nieto, E.D., Ferreira, A.M.G., Funning, G., Gabriel, A.-A., Hendrickx, M., Kafka, A.L., Keiding, M., Kerby, J., Khan, S.A., Dideriksen, A.K., Lamb, O.D., Larsen, T.B., Lipovsky, B., Magdalena, I., Malet, J.-P., Myrup, M., Rivera, L., Ruiz-Castillo, E., Wetter, S., Wirtz, B., 2024. A rockslide-generated tsunami in a Greenland fjord rang earth for 9 days. Science 385, 1196–1205. https://doi.org/10.1126/science.adm9247.

Takemura, S., Okuwaki, R., Kubota, T., Shiomi, K., Kimura, T., Noda, A., 2020. Centroid moment tensor inversions of offshore earthquakes using a three-dimensional velocity structure model: slip distributions on the plate boundary along the Nankai trough. Geophys. J. Int. 222, 1109–1125. https://doi.org/10.1093/gji/ggaa238.

Tape, W., Tape, C., 2012. A geometric setting for moment tensors. Geophys. J. Int. 190, 476–498. https://doi.org/10.1111/j.1365-246X.2012.05491.x.

Tarantola, A., 2005. Inverse Problem Theory and Methods for Model Parameter Estimation, Other Titles in Applied Mathematics. Society for Industrial and Applied Mathematics. https://doi.org/10.1137/1.9780898717921.

Tarantola, A., Valette, B., 1982. Inverse problems = quest for information. J. Geophys. 50, 159–170.

Tauzin, B., Phạm, T.-S., Tkalčić, H., 2019. Receiver functions from seismic interferometry: a practical guide. Geophys. J. Int. 217, 1–24. https://doi.org/10.1093/gji/ggz002.

Thurin, J., Modrak, R., Tape, C., McPherson, A.M., Rodríguez-Cardozo, F.R., Kintner, J., Ding, L., Liu, Q., Braunmiller, J., 2025. MTUQ: a framework for estimating moment tensors, point forces, and their uncertainties. Geophys. J. Int. 241, 1373–1390. https://doi.org/10.1093/gji/ggaf080.

Tromp, J., Komattisch, D., Liu, Q., 2008. Spectral-element and adjoint methods in seismology. Commun. Comput. Phys. 3, 1–32.

Tsai, V.C., Ekström, G., 2007. Analysis of glacial earthquakes. Case Rep. Med. 112. https://doi.org/10.1029/2006JF000596.

Tsai, V.C., Nettles, M., Ekström, G., Dziewoński, A.M., 2005. Multiple CMT source analysis of the 2004 Sumatra earthquake. Geophys. Res. Lett. 32, 2005GL023813. https://doi.org/10.1029/2005GL023813.

Turner, A.R., Ferreira, A.M.G., Berbellini, A., Brantut, N., Faccenda, M., Kendall, E., 2022. Across-slab propagation and low stress drops of deep earthquakes in the Kuril subduction zone. Geophys. Res. Lett. 49, e2022GL098402. https://doi.org/10.1029/2022GL098402.

Vackář, J., Burjánek, J., Gallovič, F., Zahradník, J., Clinton, J., 2017. Bayesian ISOLA: new tool for automated centroid moment tensor inversion. Geophys. J. Int. 210, 693–705. https://doi.org/10.1093/gji/ggx158.

Valentine, A.P., Sambridge, M., 2023. Emerging directions in geophysical inversion. In: Applications of Data Assimilation and Inverse Problems in the Earth Sciences. Cambridge Univ. Press.

Valentine, A.P., Trampert, J., 2012. Assessing the uncertainties on seismic source parameters: towards realistic error estimates for centroid-moment-tensor determinations. Phys. Earth Planet. Inter. 210–211, 36–49. https://doi.org/10.1016/j.pepi.2012.08.003.

Valentine, A.P., Woodhouse, J.H., 2010. Approaches to automated data selection for global seismic tomography: approaches to automated data selection. Geophys. J. Int. 182, 1001–1012. https://doi.org/10.1111/j.1365-246X.2010.04658.x.

Vallée, M., 2013. Source time function properties indicate a strain drop independent of earthquake depth and magnitude. Nat. Commun. 4, 2606. https://doi.org/10.1038/ncomms3606.

Vallée, M., Douet, V., 2016. A new database of source time functions (STFs) extracted from the SCARDEC method. Phys. Earth Planet. Inter. 257, 149–157. https://doi.org/10.1016/j.pepi.2016.05.012.

Vallée, M., Charléty, J., Ferreira, A.M.G., Delouis, B., Vergoz, J., 2011. SCARDEC: a new technique for the rapid determination of seismic moment magnitude, focal mechanism and source time functions for large earthquakes using body-wave deconvolution. Geophys. J. Int. 184, 338–358. https://doi.org/10.1111/j.1365-246X.2010.04836.x.

Vasyura-Bathke, H., Dettmer, J., Steinberg, A., Heimann, S., Isken, M.P., Zielke, O., Mai, P.M., Sudhaus, H., Jónsson, S., 2020. The Bayesian earthquake analysis tool. Seismol. Res. Lett. 91, 1003–1018. https://doi.org/10.1785/0220190075.

Vasyura-Bathke, H., Dettmer, J., Dutta, R., Mai, P.M., Jónsson, S., 2021. Accounting for theory errors with empirical Bayesian noise models in nonlinear centroid moment tensor estimation. Geophys. J. Int. 225, 1412–1431. https://doi.org/10.1093/gji/ggab034.

Vavryčuk, V., Kühn, D., 2012. Moment tensor inversion of waveforms: a two-step time-frequency approach: moment tensor inversion of waveforms. Geophys. J. Int. 190, 1761–1776. https://doi.org/10.1111/j.1365-246X.2012.05592.x.

Veitch, S.A., Nettles, M., 2012. Spatial and temporal variations in Greenland glacial-earthquake activity, 1993–2010. Case Rep. Med. 117. https://doi.org/10.1029/2012JF002412.

Viltres, R., Nobile, A., Vasyura-Bathke, H., Trippanera, D., Xu, W., Jónsson, S., 2021. Transtensional rupture within a diffuse plate boundary zone during the 2020 mw 6.4 Puerto Rico earthquake. Seismol. Res. Lett. 93, 567–583. https://doi.org/10.1785/0220210261.

Wang, X., Zhan, Z., 2020. Moving from 1-D to 3-D velocity model: automated waveform-based earthquake moment tensor inversion in the Los Angeles region. Geophys. J. Int. 220, 218–234. https://doi.org/10.1093/gji/ggz435.

Wéber, Z., 2009. Estimating source time function and moment tensor from moment tensor rate functions by constrained L_1 norm minimization. Geophys. J. Int. 178, 889–900. https://doi.org/10.1111/j.1365-246X.2009.04202.x.

Wehner, D., Blom, N., Rawlinson, N., Daryono, Böhm, C., Miller, M.S., Supendi, P., Widiyantoro, S., 2022. SASSY21: a 3-D seismic structural model of the lithosphere and underlying mantle beneath Southeast Asia from multi-scale adjoint waveform tomography. J. Geophys. Res. Solid Earth 127. https://doi.org/10.1029/2021JB022930 e2021JB022930.

Woodhouse, J.H., 1974. Surface waves in a laterally varying layered structure. Geophys. J. Int. 37, 461–490. https://doi.org/10.1111/j.1365-246X.1974.tb04098.x.

Woodhouse, J.H., Dziewoński, A.M., 1984. Mapping the upper mantle: three-dimensional modeling of earth structure by inversion of seismic waveforms. J. Geophys. Res. Solid Earth 89, 5953–5986. https://doi.org/10.1029/JB089iB07p05953.

Xu, C., Zhang, Y., Hua, S., Zhang, X., Xu, L., Chen, Y., Taymaz, T., 2023. Rapid source inversions of the 2023 SE Türkiye earthquakes with teleseismic and strong-motion data. Earthq. Sci. 36, 316–327. https://doi.org/10.1016/j.eqs.2023.05.004.

Yagi, Y., Fukahata, Y., 2011. Introduction of uncertainty of Green's function into waveform inversion for seismic source processes: uncertainty of Green's function in inversion. Geophys. J. Int. 186, 711–720. https://doi.org/10.1111/j.1365-246X.2011.05043.x.

Ye, L., Kanamori, H., Avouac, J.-P., Li, L., Cheung, K.F., Lay, T., 2016. The 16 April 2016, M7.8 (M7.5) Ecuador earthquake: a quasi-repeat of the 1942 M7.5 earthquake and partial re-rupture of the 1906 M8.6 Colombia–Ecuador earthquake. Earth Planet. Sci. Lett. 454, 248–258. https://doi.org/10.1016/j.epsl.2016.09.006.

Yin, J., Li, Z., Denolle, M.A., 2021. Source time function clustering reveals patterns in earthquake dynamics. Seismol. Res. Lett. 92, 2343–2353. https://doi.org/10.1785/0220200403.

Zahradník, J., Sokos, E., 2025. ISOLA2024: assessing and understanding uncertainties of full moment tensors. Seismol. Res. Lett. https://doi.org/10.1785/0220240420.

Zhan, Z., Kanamori, H., Tsai, V.C., Helmberger, D.V., Wei, S., 2014. Rupture complexity of the 1994 Bolivia and 2013 Sea of Okhotsk deep earthquakes. Earth Planet. Sci. Lett. 385, 89–96. https://doi.org/10.1016/j.epsl.2013.10.028.

Zhao, L., Chen, P., Jordan, T.H., 2006. Strain green's tensors, reciprocity, and their applications to seismic source and structure studies. Bull. Seismol. Soc. Am. 96, 1753–1763. https://doi.org/10.1785/0120050253.

Zhao, L.-S., Helmberger, D.V., 1994. Source estimation from broadband regional seismograms. Bull. Seismol. Soc. Am. 84, 91–104. https://doi.org/10.1785/BSSA0840010091.

Zhu, L., Helmberger, D.V., 1996. Advancement in source estimation techniques using broadband regional seismograms. Bull. Seismol. Soc. Am. 86, 1634–1641. https://doi.org/10.1785/BSSA0860051634.

Zhu, L., Zhou, X., 2016. Seismic moment tensor inversion using 3D velocity model and its application to the 2013 Lushan earthquake sequence. Phys. Chem. Earth (Pt A B,C) 95, 10–18.